ERYTHROSENSORS CELLULAR CHARACTERIZATION

A Dissertation

by

SANDRA CATALINA BUSTAMANTE LOPEZ

Submitted to the Office of Graduate and Professional Studies of
Texas A&M University
in partial fulfillment of the requirements for the degree of

DOCTOR OF PHILOSOPHY

Chair of Committee,	Alvin T. Yeh
Co-Chair of Committee,	Kenith E. Meissner
Committee Members,	Kristen C. Maitland
	Arum Han
Head of Department,	Anthony Guiseppi-Elie

August 2017

Major Subject: Biomedical Engineering

ABSTRACT

For diabetics, continuous glucose monitoring, and the resulting tighter control of glucose levels, ameliorates serious complications from hypoglycemia and hyperglycemia. Today, diabetics measure their blood glucose levels multiple times a day by finger pricks, or use implantable monitoring devices. Still, glucose and other analytes in the blood fluctuate throughout the day and the current monitoring methods are invasive, immunogenic, and/or present biodegradation problems. Using carrier erythrocytes loaded with a fluorescent sensor, we seek to develop a biodegradable, efficient, and potentially cost effective method for long-term monitoring of blood analytes. We aim to reintroduce sensor-loaded erythrocytes to the bloodstream and conserve the erythrocytes lifetime of 120 days in the circulatory system.

Here, the efficiency of two loading procedures is compared. Hypotonic dilution employs hypotonic buffer to create transient pores in the erythrocyte membrane, allowing dye entrance and a hypertonic buffer to restore tonicity. Electroporation relies on controlled electrical pulses that results in reversible pores formation to allow cargo entrance. As part of the cellular characterization of loaded erythrocytes, size and hemoglobin content was evaluated. Cell recovery and fluorescence per cell measurements also render optimal loading conditions. Furthermore, AFM and confocal microscopy protocols were implemented to evaluate morphological changes induced by hypotonic dilution. The development of a suitable protocol to engineer carrier erythrocytes has profound and lasting implications in the erythrocytes' lifespan and sensing capabilities.

ACKNOWLEDGEMENTS

I would like to offer my sincere gratitude to my committee co-chairs Professor Kenith Meissner, and Professor Alvin Yeh. I also want to thank my committee members, Professor Kristen Maitland, and Professor Arum Han. Thank you for the challenging discussions, and everything else in between. This has been an intense learning period for me.

To my lab mates and colleagues: Sarah Ritter, Ansam Talib, Jake Carrow, Chi-heng "Martin" Wu, Andrea Locke, Rachel Unruh, Erica Hord, Yil-Hwan You, Steve Zambrano, Pauline Luong, Nicholas Cooley, thank you for your support and continuous encouragement. My sincere thanks also goes to our collaborators Professor Mark Milanick and Professor Timothy Glass for their continuous guidance throughout the project.

I would like to thank my parents, Nicolas William Bustamante, and Maria Marleny Lopez Guerra for guiding me throughout my life in science and non-science stuff. I would also like to thank my friends and family for their encouragement.

Finally, I want to thank my husband, Jersson Emir Placido Escobar for his unconditional love, patience and support, "Yo te amo más!" This accomplishment would not have been possible without them. Thank you.

CONTRIBUTORS AND FUNDING SOURCES

Contributors

This work was supported by a dissertation committee consisting of advisor Professor Alvin T. Yeh, co-advisor Kenith E. Meissner and Professor Kristen C. Maitland of the Department of Biomedical Engineering and Professor Arum Han of the Department of Electrical and Computer Engineering. All work conducted for the dissertation was completed by the student independently.

Funding Sources

This work has been possible thanks to the NIH support, the Texas A&M diversity fellowship and the Alfred P. Sloan foundation fellowship. Also, I would like to acknowledge the International Society for Optics and Photonics proceedings (SPIE) for reprint permission and the Biomedical Engineering Society (BMES) for travel support.

TABLE OF CONTENTS

Page

LIST OF FIGURES

Page

LIST OF TABLES

Page

CHAPTER I

INTRODUCTION

In the United States, approximately 30 million people have diabetes and 87 million more have prediabetes. Thus, a third of the country's population could become diabetics in the coming years [1,2]. Diabetes occurs when insulin insufficiency and/or cells unresponsive to insulin induce a rise of glucose levels in the blood. Irregular blood glucose level is a medical condition that requires accurate, continuous and long-term monitoring. Diabetics rely on the arduous task of maintaining normal glucose levels using costly, and complicated procedures. The regimen for most diabetics includes self-monitoring glucose levels multiple times a day using a fingerstick with a glucose meter, or an implantable continuous glucose monitoring system. Among other issues, common glucose meters' accuracy are prone to human error, dependent on the meter and strip quality, and susceptible to interfering factors [3-6]. Longstanding concerns of implantable glucose monitoring devices are their immunogenicity and problems related to toxicity, selectivity and biodegradation [7-10]. Major complications arising from improper diabetes care include: blindness, renal disease, leg amputations and even death [11,12]. Furthermore, the lack of continuous glucose monitoring leaves diabetics vulnerable to complications such as hypoglycemia and hyperglycemia, which can lead to death. Diabetes incidence, prevalence, and mortality reveal the magnitude of the global burden and the need for a biocompatible, biodegradable, and potentially cost effective strategy to monitor continuously and for a long-term blood analytes. Erythrocytes loaded with a fluorescent analyte-sensitive dye (erythrosensors) can be detected using a light source through the

skin with the signal used for continuous monitoring of blood analytes, such as glucose [13-17].

Glucose meters use electrochemical principles to measure blood glucose. Glucose oxidase converts glucose into glucolactone and oxygen into hydrogen peroxide. Clarke and Lyons first described an amperometric enzyme biosensor [18,19]. The enzyme electrode strip measures depletion or increase of reactant to indirectly correlate glucose concentration in a blood sample. Despite enzyme sensitivity and selectivity for glucose, difficulties arose pertaining operator errors which plagued the meter accuracy.

Nowadays fingerstick-based glucose meters require a user to draw a blood sample by finger pricking, collect a blood drop on a sample strip, and read the glucose level measurement from a glucose meter [20,21]. The patient sparsely monitors blood glucose levels pre and post-prandial. Misuse of the glucose meter (improper calibration, poor blood sample, contamination etc.) and inadequate patient compliance disturb the accuracy of the glucose meter readings [22]. Moreover, sparse monitoring by finger pricking throughout the day, instead of continuous monitoring of glucose levels, hinders the construction of accurate trends and increases the risk of complications [3,4]. Continuous or near continuous measurements reduce the risk of serious complications resulting from either hypoglycemia (i.e. coma and death) or hyperglycemia (i.e. kidney failure, heart disease, gangrene, etc.) [23].

The implementation of implantable continuous glucose meters (CGM) improve blood glucose levels monitoring and reduce the incidental hypoglycemia/hyperglycemia by providing real-time measurements. However this subcutaneously device also bear a new set of problems [24]. Both biochemical and cell-based devices have failed to address issues such as immunogenicity, intracutaneous reactivity, toxicity, selectivity and biodegradation [25,26]. Furthermore, current approved devices are limited to monitoring blood sugar levels for up to 7 days. Another drawback is susceptibility to malfunction due to patient physical activity and glucose level variability throughout the circulatory system [27,28]. A major concern lies on the fact that, over time, implantable continuous glucose devices tend to trigger an undesirable immune response; rapid recruitment of monocytes and macrophages signals the formation of a thick fibrotic capsule which physically and physiologically separates the device from blood vessels [29]. This separation can lead to inaccuracy and shortens lifetime. The lack of vasculature creates niches susceptible to infection, and variability in glucose level readings due to implant isolation [7,29,30]. Implantable glucose monitoring devices have improved self-monitoring of diabetes, but these devices' long-term biocompatibility, and accuracy are still disputed [31-33].

Diabetes and other debilitating conditions can be diagnosed, treated and/or monitored by blood sampling. Blood testing stands as the most common procedure for health care. Because numerous medical conditions affect or are affected by the blood, it is the norm to use blood testing for the analysis of biochemical, toxicological and

immunological studies among others. Thus, the importance of exploring alternative long-term blood monitoring.

Given its public health importance, this work lays the foundations for the characterization of a novel alternative to manage diabetes. Diabetes self-management could change from multiple daily finger pricks to a doctor's visit every three months to infuse erythrosensors, analyze trends, and implement a plan to manage the disease. It could also allow the prediction of events that significantly alter the glucose levels within the patient's habits. Circulating erythrosensors could help reduce or prevent complications by alerting patients of life-threatening events such as hypoglycemia and hyperglycemia [7]. A compelling benefit lies in erythrosensors' ability to provide continuous data to assist physicians and patients in making better care decisions.

Erythrocytes' unique property of acting as a biocompatible carrier system can be exploited in biosensing [13]. Thanks to their circulation in the bloodstream, continuous monitoring could be achieved. The use of erythrocytes as an *in-vivo* biosensor dubbed erythrosensors, could improve diabetes care by reducing the burden of monitoring blood glucose throughout the day since carrier erythrocytes can circulate in the blood for up to three months [14]. Erythrosensors could address the need for an accurate, biocompatible, long-term blood-analyte monitoring platform.

Erythrocytes

In 1674, Lee Van Hock first described the microscopic characteristics of red blood cells also known as erythrocytes. The most abundant cells in humans, erythrocytes form in the bone marrow. One of blood's major constituents along with plasma, white blood cells and platelets, erythrocytes' primary job is to transport oxygen and carbon dioxide. Their characteristic biconcave-disc form maximizes their surface area for oxygen transport and exchange. However, these enucleated cells preserve key properties, such as size, volume and levels of hemoglobin, as they transit throughout the circulatory system. Erythrocytes navigate the circulatory system transporting molecules while maintaining their physiological properties. Having no internal organelles, erythrocytes rely on anaerobic glycolysis to generate energy. Erythrocytes' ability to pull and squeeze through the circulatory system plays a key role in their life span.

Mammalian erythrocytes maintain a constant volume despite severe deformation during circulation through capillaries. Bovine erythrocytes are approximately 5 μm in diameter, rat erythrocytes are approximately 6 μm in diameter and human erythrocytes are approximately 8 μm in diameter. However, the erythrocyte characteristic shape is flexible and the biconcave disk deforms to navigate through the smallest capillaries. These deformations depend of the diameter of the capillary and flow rate [34]. The "simple" architecture of erythrocytes is in fact a complex network of mechanical, chemical and biological interactions [16,35]

Aging cells display changes in size and morphology. These changes imply abnormalities in the cytoskeleton, membrane, motor/adhesive complexes and/or secondary reasons including precipitation of hemoglobin [36]. It is known that aging erythrocytes deform, often into spherocytes, and become more rigid, which interferes with their ability to circulate in the bloodstream. Ultimately, senescent erythrocytes are taken out of circulation via phagocytosis in the lymphoid organs.

The erythrocyte membrane flexibility is dependent upon the cell cytoskeleton. A phospholipid bilayer, transmembrane proteins and membrane-associated proteins construct the erythrocyte membrane. The cytoskeleton is composed mainly of an intrinsic network of spectrin protein, which attaches to other transmembrane proteins [37]. These molecular interactions constitute the framework for the collective mechanical and chemical functions of the cell membrane and the cytoskeleton. The functions range from ion transportation across the membrane to cell-cell signaling. The cytoskeleton and cell membrane have a cooperative role in the behavior and properties of erythrocytes including the size and shape [36].

Study of subcellular architecture has revealed difference between pathological and normal erythrocytes. Kamruzzahan et al. developed an anchoring technique to investigate erythrocytes shape from normal donors and patients suffering from systemic lupus erythematous (SLE) using atomic force microscopy (AFM). SLE is an autoimmune disease in which antibodies signal erythrocytes phagocytosis. Patients with SLE exhibit

spherical deformations, corrugations and holes in the erythrocyte morphology when compared to erythrocytes from healthy volunteers [38]. The resulting topographical images of immobilized and fixed human erythrocytes from healthy and disease patients showed morphological differences. This study described the immobilization of erythrocytes and produced AFM topographical images comparing healthy and pathological erythrocytes.

Carrier erythrocytes and erythrocyte inspired delivery systems

Known as pink, resealed, carrier and/or ghost erythrocytes/red blood cells, these cells form when native erythrocytes undergo osmotic, chemical, electrical, or reprogramming treatment and are loaded with exogenous cargo. There are a number of established methods to load erythrocytes with cargo, thus creating carrier erythrocytes. The hypotonic hemolysis technique relies on a hypotonic medium to drive the erythrocyte to a pre lysis point and load cargo [39]. Hypotonic dilution, is based on diluting erythrocytes in a lysis solution with the cargo to be entrapped [13]. Hypotonic dialysis is similar to hypotonic dilution, but it uses a dialysis tube filled with erythrocytes, and immersed in a hypotonic lysis solution to allow cargo to diffuse through the dialysis membrane for entrapment [40]. Stepwise hypotonic pre-swelling of erythrocytes in increasing hypotonic solutions to swell and allow cargo diffusion, is another method to load erythrocytes [41]. Erythrocytes can also be loaded using chemical perturbation through exposure to polygenic antibiotics [42]. In addition, loading of drugs/substances through electric break down or electroporation has been reported to open up pores with

diameters depending on the charge used, allowing cargo entry [43,44]. Recently, the use of erythrocyte membrane-derived erythrosensors as drug delivery vehicles and the genetically programming of erythroblast to express surface proteins in the erythrocyte membrane have been explored because of their biocompatibility and biodegradability [45].

A common method for preparation of carrier erythrocytes is via hypotonic dilution. Placing erythrocytes under hypotonic conditions swells the cells and leads to membrane poration. The regulation of internal and external molecules concentration allows the cargo to diffuse when reversible pores form and the cell attempts to equilibrate with the environment [13,14]. Restoring the homeostatic condition, reseals the pores encapsulating drugs, enzymes or molecules of interest, in this case a fluorescent dye.

Fueled by the advances in loading procedures, there has been a steady implementation of carrier erythrocytes in the drug delivery field (Table 1). The use of erythrocytes to transport molecules began almost 50 years ago [16,46]. Carrier-erythrocytes provide prolonged circulation, high encapsulation efficiency, and reticuloendothelial system (RES) targeting when compared with biomaterials for drug delivery [47-53]. Although, a carrier Erythrocyte system targeting RES is now in preclinical trails, a latent problem is maintaining the integrity of the properties that made erythrocytes attractive in the first place [50].

Table 1. Suitable techniques to load cargo into erythrocytes

Technique	RBC	Cargo	Efficiency	Ref.
Hypotonic Hemolysis	Human	FITC-dextran/FITC-Lysozyme	27–31%	[54]
Hypotonic Hemolysis	Human	Antisense oligodeoxynucleotide	8-10%	[55]
Hypotonic Hemolysis	Rat	Bovine serum albumin	2%	[56]
Hypotonic Dilution	Frog	Taurine	N/A	[57]
Hypotonic Dilution	Human	Myo-[3H]-inositol	14%	[58]
Hypotonic dialysis	Rat	Antiretroviral Zidovudine	30%	[59]
Hypotonic dialysis	Rat	Amikacin	N/A	[60]
Hypotonic dialysis	Mice	Etoposide	9.5%	[61]
Hypotonic dialysis	Mice	Glutamate dehydrogenase	56%	[62]
Hypotonic Pre-swelling	Human	Interferon-α 2β	14.5%	[63]
Hypotonic Pre-swelling	Human	Bovine serum albumin	30%	[63]

Carrier erythrocytes have also been studied for the transport of contrast agents and standards for imaging and cytometry applications. Doberstein et al. described erythrocytes loaded with dextran and rhodamine as standards for flow cytometry [64]. The finding suggests that the dextran-loaded erythrocytes had comparable fluorochrome content to that of commercially available microbeads for flow cytometry standards. Although, it is not clear if the fluorescent molecules were encapsulated in the erythrocytes or associated with the membrane. In recent years, there has been an increasing amount of literature on the application of nanoparticles-loaded erythrocytes for imaging. One study by Sungsook et al., examined the loading of gold nanoparticles (AuNPs) using the hypotonic dilution technique for dynamic x-ray imaging of blood flow. The results showed AuNPs aggregate with carrier erythrocytes to act as a contrast agent/flow tracer and enhance dynamic X-ray imaging [65]. To the best of our knowledge, the only work on AFM imaging of carrier erythrocytes was done to evaluate erythrocytes loaded with superparamagnetic iron oxide

nanoparticles (SPIONs) for MRI imaging [66]. Despite maintaining an average size, the topographical images of erythrocytes carrying SPIONS revealed a rugged surface. In addition, the height profile of the carrier erythrocyte reached around 70 nm and displayed collapsed membranes. Collectively, these studies outline the role of carrier erythrocytes in other biomedical applications. These studies also highlight the need to understand the physical properties of carrier erythrocytes.

Despite the advantages of using carrier erythrocytes, little is known about how the physical properties contribute to prolonged circulation, slower drug release rate and eluding the immune system recognition. For instance, it has been reported that increased stiffness halts erythrocytes ability to squeeze through capillaries and can cause clogging [67]. Moreover, reports of carrier erythrocyte rapid clearance and phagocytosis have limited their implementation in other applications [41]. The membrane poration and the loss of hemoglobin during loading process, could lead to irreversible cellular changes, immune system recognition and premature clearance.

Recent studies have raised concerns about the external adverse effects on transfused erythrocytes. Storage lesion, improper sample handling, and blood-borne diseases are a few of the challenges, the implementation of carrier erythrocytes face [68-70]. Conserving erythrocytes physiological characteristics could improve the yield, integrity and the performance of carrier erythrocytes.

To address the limitations of carrier erythrocytes researchers are bridging the gap between synthetic and biological systems. A previous study reported nanoparticles linked to erythrocyte membranes [71-74]. Researchers found increased circulation time (up to 10 hours) for *in-vivo* for nanoparticles non-covalently attached to the erythrocyte membrane, but it was feared that shear stress in capillaries could detach the nanoparticles from the erythrocyte in the long-term. A number of researchers have also reported biomimetic PLGA and PEG particles, which resemble erythrocyte morphology and function [72,74]. The biomimetic PLGA and PEG particles were engineered to have cellular properties similar to erythrocytes. The PLGA-RBCs displayed similar mechanical properties and oxygen-carrying capabilities while the PEG-RBCs rendered a tunable elasticity, which allowed them to circulate for a period of time similar to native erythrocytes [73]. To improve drug delivery, researchers used erythrocytes as nanoparticles transporters and created particles that mimic erythrocyte shape.

Erythrosensors

Erythrocytes can transport a number of small molecules and biological agents, including sensing probes. Milanick et al. dubbed carrier erythrocytes (red cell ghosts) encapsulating an optical sensor, erythrosensors. Erythrosensors intend to provide long-term and continuous measurements of extracellular analytes in the blood. After functionalization, erythrocytes carrying fluorescent sensors are transfused to the host animal or patient to monitor plasma analyte concentrations non-invasively via fluorescent detection. Conserving erythrocyte lifespan, erythrosensors could circulate in the

bloodstream for up to 120 days. The long-term goal is to automate the blood sampling, erythrocytes isolation, cargo loading, and erythrosensors resealing. One major drawback of this approach is that still requires a periodical blood sample, although not as often as using the fingerstick monitoring method for glucose, for example.

To date, hypotonic dialysis and hypotonic dilution have been studied to generate erythrosensors. Both methods rely on an osmolarity change to cause membrane disruption. Hypotonic dialysis relies on a time-consuming diffusion exchange of higher osmolarity buffer to lower osmolarity buffer through a dialysis membrane and subsequently changing the osmolarity in the erythrocyte environment gradually. Hypotonic dilution is a method where erythrocytes are quickly diluted in a hypotonic buffer causing membrane lysis. Although both methods produced a number of fluorescent dye loaded erythrocytes (>50%), one major drawback has been that the resulting population had varying amount of dye loaded, and some resulting erythrosensors seem to have no dye loaded at all. Throughout this dissertation the terms non-uniform dye loading will be used to refer to the varying amount of dye loaded among a population of erythrosensors, where a portion of the erythrosensors appear to carry more dye than others.

In a first study, sheep erythrocytes were subject to the hypotonic dialysis at 0°C, and subsequently washed and suspended in an isotonic solution to restore isotonic osmolarity. Fluorescence imaging revealed a loading efficiency >50% and non-uniformly dye loading among the population of erythrosensors [14]. Then, a theory to overcome

fluorescent detection of a non-uniformly dye loaded erythrosensors population was described, and a ratiometric approach for *in-vivo* work was recommended.

An alternative loading process was then evaluated. Hypotonic dilution loading removes most of the hemoglobin of the erythrocyte. This method consists of placing erythrocytes in hypotonic solution at 0°C to create pores and quickly seal the membrane using a hypertonic buffer and 37°C incubation. The fluorescent micrographs revealed ~50% loading efficiency, matching previous studies [13]. In addition, the emission spectrum of erythrosensors loaded with fluorescein isothiocyanate conjugated with glycylglycine (FITC-glygly) was shown to be equivalent to the emission by free FITC-glygly. The most striking result from this study is the extracellular pH tracking by the erythrosensors loaded with a pH sensitive dye. The results demonstrated the idea that uniform dye loading is not required for pH sensing purposes [13]. However, neither carrier erythrocyte nor erythrosensor cellular properties are yet fully understood.

A latent problem with erythrosensors lies in the innate heterogeneity of the initial erythrocyte population. Here the term heterogeneity is used to describe the different erythrocytes life cycles stages while in circulation (i.e. reticulocyte vs. mature erythrocytes). Reticulocyte mature into mature erythrocytes after 24-48 hours of entering the blood stream. Normal mature human erythrocytes live for approximately 120 days. Thus, not only is it necessary to consider the fate of aged erythrocytes, but also the fact that at any given moment the erythrocyte population of a blood sample contains

reticulocytes, and mature erythrocytes undergoing different cell cycle-related molecular modifications. Moreover, every second millions of new erythrocytes replace aged erythrocytes and will dilute erythrosensors in circulation [14]. In addition, physical activity, such as exercising, causes hypoxia to promote erythropoietin and subsequently erythrocyte production. This biological processes could impact the production of erythrosensors, and their circulation and sensing abilities. Using the 1-3% circulating reticulocytes to produce erythrosensors could address some of the issues related to the population heterogeneity; however, this work lies beyond the scope of this thesis.

For long-term *in-vivo* sensing erythrosensors must first evade premature immune system recognition upon entering circulation. Ideally, after undergoing the loading process, erythrosensors would maintain the erythrocytes' biochemical properties that signal self, such as the membrane protein CD47. Changes in the erythrocyte membrane's integrity, flexibility and chemical composition would result in immune system detection and/or clearance in the spleen or by macrophages. However, erythrocyte membrane changes caused by loading procedures remain unknown. Furthermore carrier erythrocytes or erythrosensors cellular properties are not fully understood.

This work focuses on four key features for optimal erythrosensor performance: hemoglobin content, size, morphology and uniform loading. Erythrocyte life span depends on a variety of physical properties. Erythrosensors must maintain near-normal hemoglobin level in order to preserve erythrocytes morphology, function within the circulatory system

and avoid immune system detection. Erythrocyte morphology is well understood. Thus, comparing erythrocyte and erythrosensor morphology could work as an indicator of viability. Albeit, theoretical work indicates that using non-uniform dye loaded erythrosensors does not alter the signal detection, uniform dye loaded erythrosensors not only simplifies the fluorescent signal detection but also efficiently exploits a donor's erythrocyte sample [13].

Chapter II introduces the methods used. Chapter III presents methods for erythrocyte loading with the model cargo fluorescent FITC-glygly that maximize the fluorescent signal. Dilution of erythrocytes in a hypotonic buffer and electroporation, application of small electrical charges to the erythrocyte, are evaluated [13,43,75,76]. While these loading procedures are used for drug delivery, this work combines loading a fluorescent dye as a sensor and using an erythrocyte as the sensor carrier.

In pursuit of establishing reliable methodology to understand the physiological changes that erythrocytes undergo when converted into erythrosensors, non-uniform dye loaded erythrosensors produced via hypotonic dilution were explored. Different fluorescent dyes were used and morphological changes in erythrosensors were characterized. Two fundamental topics were investigated: the carrying capabilities and the cellular changes in erythrosensors made using the optimized hypotonic dilution procedure.

A procedure to uniformly load erythrocytes with fluorescent dyes while maintain intrinsic cell functions is essential for the survival of the erythrosensors *in-vivo*. In an effort to decrease recognition by the immune system, and achieve prolonged circulation time, chapter IV describes a simpler and faster swelling-based loading procedure. The FDA approved dye idocyanine green is studied for retinal imaging. The evaluation of erythrosensor population cellular properties pave the way for *in vivo* applications.

The unique disk-like shape permits erythrocytes to squeeze throughout the circulatory system. For sensing applications, the fluorescent signal emitted through the complex physiology of the cell membrane, tissues and skin, pay a key role for detection. For erythrosensors to circulate in the blood stream undetected our goal is to maintain the intrinsic characteristics of erythrocytes, while maximizing the fluorescent signal intensity. Hypotonic dilution and a swelling method were evaluated to load erythrocytes with fluorescent FITC-glygly focusing on the size, shape and the fluorescent signal emitted by the FITC-glygly loaded erythrocytes.

Final remarks in chapter V include a summary of the work, the limitations and outlook. The long-term goal is to optimize carrier erythrocytes with fluorescent dyes as continuous glucose erythrosensors. Creating a model system towards *in-vivo* cell-based sensing, to avoid conventional glucose meters and/or blood sampling: an adaptable technology for long-term monitoring which can avoid the sentinel cells of the human immune system.

CHAPTER II

METHODS

The focus of this work was to investigate changes to key erythrocyte properties after loading, optimize alternative procedures, and generate uniformly loaded erythrocytes. Rat blood samples were collected into CDPA anticoagulant. Whole blood samples were centrifuged at 12,000 ×g for 5 minutes, and the plasma and white blood cells were removed. The cells were washed with 165 mM NaCl. Bovine blood was collected into CDPA anticoagulant and gentamicin container and washed before procedures. Fluorescent fluorescein isothiocyanate (FITC), as model cargo, was obtained from Sigma Aldrich (46950 Sigma). Two widely used loading protocols were explored for loading erythrocytes: electroporation and hypotonic dilution. Both methods create pores in the cell membrane to allow cargo entrance, and use a 37° C incubation and a buffer to restore the cell membrane [13,14,42]. However, electroporation relies on electrical charges, while hypotonic dilution makes use of a hypotonic buffer to create the reversible pores. A preswelling method was develop, towards maintaining the erythrocyte cellular properties.

Electroporation

The temperature of packed erythrocytes was lowered to 0° C. Electroporation 0.2 cm cuvettes for 400 µl samples were used. Electroporation was performed using a Bio-rad Gene Pulser Xcell™ system at 250, 300 and 750 V with a square wave pulse ranging from 0.5 to 5 ms, and intervals of 15 minutes for a total of four cycles. Cells were incubated for 10 minutes at 4° C, and diluted 1:2 in resealing solution consisting of 8 mM KCL (P9541-

Sigma), 150 mM NaCl (s9888-Sigma), 6 mM NaH2PO4 (s5011-Sigma), 10 mM D-Glucose (g8270-Sigma), 2 mM magnesium chloride (MgCl2 M8266-Sigma), 1% BSA, pH 7.4. Resealing was achieved by incubation at 37°C for 1 hour and at 4°C for 24 hours. Loaded erythrocytes were washed with phosphate buffer saline (PBS) by centrifugation and stored at 50% hematocrit in ice (4°C) [43,75,76]. Control cell for the experiment were electroporated at 300 V amplitude and 1 ms pulse width to account for possible auto fluorescence. In addition, a second control was prepared using naive erythrocytes at the same concentration as the samples electroporated, and placed in a cuvette with FITC-glygly but the samples were not electroporated. This control was used to determine spontaneous uptake of the fluorescent dye, if any.

Hypotonic dilution

The temperature of hypotonic lysis buffer (10x solution consisting of 10 mM $MgCl_2$, 20 mM EDTA, 50 mM phosphate buffer, 1 mM Urea) was lowered to 0-2° C and 1 ml FITC-glygly at pH 9.0 was mixed in 25 ml of 1x hypotonic lysis buffer (2.5ml of the 10X lysis buffer +22.5 ml deionized water). Packed erythrocytes (2 ml) were diluted in 25 ml aqueous lysis solution and incubated for 10 minutes. Then 2.5 ml of concentrated hypertonic lysis buffer (10x) were added followed by incubation for 10 minutes at 0° C, and then at 37° C for 30 minutes. Looking to achieve a more uniform loading, cells were gently shaken every 10 minutes for the duration of the incubation. The resultant mixture was then centrifuged; the supernatant saved for absorbance measurement, and the pellet centrifuge with 165 mM NaCl (washing solution) until supernatant was visible clear. To

eliminate FITC-glygly and debri aggregates, the sample was passed through a 40 μm membrane and suspended at 50% hematocrit (hct) in PBS.

Preswelling

Bovine whole blood in CDA anticoagulant was rinsed with Phosphate buffer solution (PBS) and the top layer of white blood cells was removed. Packed erythrocytes (1 ml) were resuspended in 1 ml of preswelling buffer, and incubated for 3-5 minutes to allow pore formation while mixing gently by inversion. FITC-glygly (5 mM FITC mixed with 20 mM glygly for 30 minute at room temperature) or ICG cargo was added and the cells were incubated for additional 5 minutes, followed by the addition of resealing solution (1.65 M KCl, 0.2 M NaCl, 33 mM NaH_2PO_4, 0.1 M Glucose, 4 mM $MgCl_2$, 1 mM Inosine, 1 mM Adenine). The sample was incubated at 37° C for 1 hour. Finally the samples was centrifuged (5-7x) at 745g for 3 minute with PBS and suspended at 50% hct (v/v) in PBS.

Fluorescence microscopy

Following encapsulation, samples were immediately imaged using a Nikon TE 2000 Epi-fluorescent microscope. Nikon Blue excitation block B-2E/C was used to excite FITC, which absorbs at 492 nm. A 5 μl sample was taken from the 50% hct sample and deposited on a microscope slide and smeared/covered with a 0.15 mm coverslip for imaging. The corrected total cell fluorescence (CTCF) was determined using randomly selected cells from each group (Electroporation 300 V and hypotonic dilution). The

average integrated density, area, and mean fluorescence background signal was used in the following equation:

CTCF = Integrated density – ([Area of cell] X [Mean fluorescence of background])

Spectrophotometry

Hemoglobin and FITC-glygly concentrations were determined using the Hitachi U-4100 UV-Vis-NIR spectrophotometer. The absorbance of hemoglobin in the supernatant was measured at 540 nm, and the absorbance for FITC was measured at 492 nm using the liquid stage. Similarly, the theoretical amount inside the erythrocytes was calculated using 100 µl samples of control erythrocytes, 100 µl of FITC-glygly cells loaded via electroporation and 100 µl of FITC-glygly cell loaded via hypotonic dilution. Samples were lysed with 900 µl deionized water (diH_2O). Absorbance measurements were recorded on the same day. Using as reference the fact that hemoglobin concentration in bovine blood ranges is 8-15 g/dl, the concentration inside control erythrocytes was calculated. Hemoglobin retained after loading was calculated using the absorbance at 540 nm of lysed samples. The resulting absorbance was multiplied by the dilution factor, and subsequently multiplied by the factor relating concentration and absorbance (cell concentration found divided by the absorbance obtained).

Confocal microscopy

Cells were fixed in 0.025% glutaraldehyde to increase mechanical strength and stability. Then a 5 µl sample was deposited on a Poly-L-Lysine (PLL) coated slide to immobilize the sample for imaging. Confocal fluorescence microscopy was performed using an Olympus FV1000 confocal microscope. A 100x objective with a 1.4 numerical aperture was used to image the fluorescence emission under 488 nm (Argon) laser excitation. Stacking in the Z-axis direction of the fluorescence images was accomplished by capturing optical slices at 0.37-0.45 µm intervals through the sample sequentially. Fluorescence was collected using a 505–575 nm filter set. Analysis and reconstruction of 3D volumetric images was achieved using the full version of Olympus confocal software. For the work creating z-stack of bovine and human erythrocytes after preswelling loading in chapter III, the Zeiss Laser Scanning Microscope (LSM) model 710 equipped with a 40X/1.3 oil objective and Zen 2010 software was used. ImageJ was used for image analysis.

Atomic force microscopy

To produce AFM topographical images of erythrosensors and naive erythrocytes, cells were fixed using 0.025% glutaraldehyde, and deposited on a Poly-L-Lysine (PLL) coated slide. The Bruker Dimension Icon AFM was used for scanning and obtaining topographical image from erythrosensors and naive erythrocytes. Ideally, when imaging cellular samples, a spherical AFM tip should be used. Because of time/funding constrains, we used a diamond tapping tip and the ScanAsyst in tapping mode to image the sample.

The scan size was 40 μm x 40 μm, the rate was 0.500Hz, and there were 512 samples/line. For the tapping mode, the Bruker tip MPP21000 RSFP 3N/m was used.

Contact mode measures topography and lateral force image/friction by scanning the probes in a raster patter on the sample surface, while monitoring the cantilever deflection. Tapping Mode refers to the oscillation of the probe near its resonance frequency and intermittently interaction with the sample surface. PeakForce Tapping is a company-developed mode where the cantilever oscillation (below resonance), results in sequential force-distance curves. ScanAsyst is an image-optimization scanning mode and works similar to PeakForce Tapping. Using ScanAsyst, the system continuously monitors image quality and makes parameters adjustments to parameters such as set point, feedback gain, and scan rate. This mode operates at lower forces than tapping mode, and uses the force curves as an imaging feedback signal. Erythrocytes are delicate samples; hence, a combination of ScanAsyst (liquid) and tapping mode (air) was used for AFM experiments to minimize force applied to the sample.

To quantify the surface roughness, the mean of the absolute vertical deviation from the mean line of the topographical profile, Ra, was calculated. Briefly, a 1 μm x 1 μm section was chosen from six different topographical images (three control RBC images and three erythrosensors images). From each cell three Ra values were calculated and averaged using the Nanoscope software version 6.14.

Image flow cytometry

For each sample, 20,000 images were collected. The template of the image flow cytometer to acquire the data, relies in calibration beads to focus the laser and to monitor the flow rate. The cell classifier function was used to avoid debris and target cells based on size. The 488nm laser power was set to 20 mW. Subsequently, the IDEAS Version 4.0 image analysis software package (Amnis) was used to analyze the data. Morphologic (circularity, and aspect ratio), dimension (area, and length,) and fluoresce intensity parameters of erythrocytes and erythrosensors loaded via the optimized hypotonic dilution or the swelling procedure were calculated using images of erythrocytes by IDEAS software.

Statistical analysis

One-way ANOVA and t tests were performed using GraphPad Prism Software version 6.00, La Jolla California, USA. The image flow cytometry data was interpreted using principal component analysis (PCA). PCA approximate visualization of the dataset by reducing the dimensionality of complex data. The dimension, morphological and fluorescent features were analyzed using SAS.

CHAPTER III

HYPOTHONIC DILUTION VS ELECTROPORATION *

This study offers insight into maximizing loading of FITC-glygly into erythrocytes by optimizing and implementing loading protocols. Erythrocyte life span depends on a variety of properties including cell size, volume, shape, surface electrical charge, and stiffness. This chapter focuses on comparing loading efficiency, hemoglobin contents and fluorescent signal of two different loading procedures: hypotonic dilution and electroporation (Figure 1).

The goal is to evaluate alternative loading procedures and minimizing changes to the erythrocyte morphology while achieving uniform dye loading using hypotonic dilution and/or electroporation. Conserving the innate erythrocyte properties in erythrosensors is a concern for erythrocyte-based sensors. Thus, questions have been raised about erythrosensors' ability to survive for prolonged biosensing based on changes to the innate erythrocyte structure. To investigate hemoglobin preservation and loading efficiency, data was drawn from two main sources: fluorescence microscopy imaging and spectrophotometry. Both hemoglobin preservation and loading efficiency must be taken into account for creating erythrosensors. Changes in hemoglobin concentration were

---

* Part of the data in this chapter is reprinted with permission from "Characterization of carrier erythrocytes for biosensing applications" Bustamante López SC, Meissner KE, 2017. Journal of Biomedical Optics, 0001; 22(9):091510, Copyright 2017 by Society of Photo-Optical Instrumentation Engineers.

analyzed using spectrophotometry for erythrocytes loaded via both, electroporation and hypotonic dilution. Statistical analysis was used to show significant differences between the concentration of hemoglobin of erythrosensors loaded via hypotonic dilution and electroporation. Confocal microscopy and AFM were used to understand erythrosensor size, morphology and uniformity of the dye loaded.

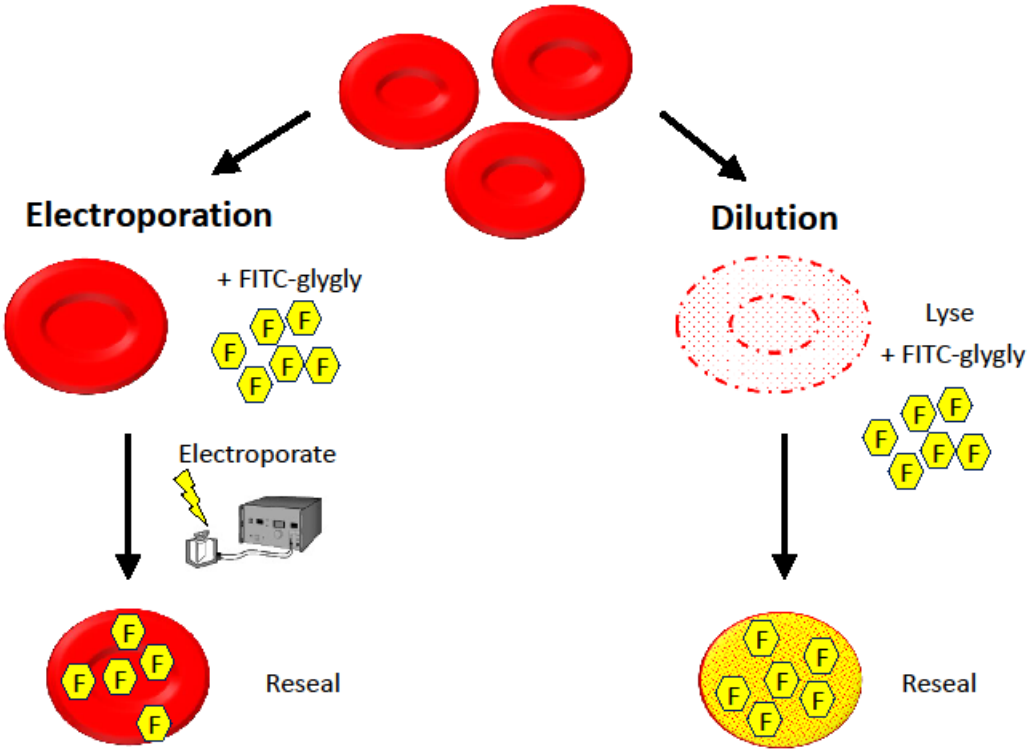

Figure 1. Electroporation vs. hypotonic dilution procedures.

Electroporation relies on short but intense electrical charges to create trans-membrane pores and allow cargo entrance [43,75,78]. Due to the membrane potential difference and reversible electric breakdown, the membrane phospholipid reassembles forming hydrophilic pores. This technique has achieved popularity for drug delivery and transformation/transfection applications because the pore size is tunable and dependable on the electroporation conditions. Proteins, nucleic acids, and particles have been encapsulated via electroporation [44,79,80]. The standard parameters for human erythrocyte loading are 300 V, 1 ms pulse time and up to 8 pulses every 15 minutes. The membrane poration is then resealed by incubation at 37°C [43]. Under optimal conditions, erythrocytes loaded using this technique have high cell recovery. In addition, the cells maintain their size and shape, and *in vivo* circulation times [75]. These attributes motivated the evaluation of electroporated erythrocytes for use as erythrosensors. The efficiency of this technique to load FITC-glygly into erythrocytes was evaluated under different conditions.

Hypotonic dilution, as indicated by the name, consists of the dilution of erythrocytes in a mix of hypotonic buffer plus the molecule to be encapsulated. This change in osmolarity creates pores or lyses the erythrocyte membrane, depending on the osmolarity, and allows cargo entrapment as erythrocytes attempt to equilibrate with the extracellular environment, in a homeostatic process [81,82]. Since erythrocytes lack mechanisms of volume control, they swell as consequence of the ion channels and transporters in the membrane that allow water permeability [83]. These membrane pores

also allow large molecules, such as FITC-glygly, to diffuse, thanks to the concentration gradient. Pore lifetimes are temperature dependent and the process is reversible. The osmotic equilibrium is restored with hypertonic buffer and resealing is achieved by incubation at 37°C. A number of procedures based on hypotonic swelling, but hypotonic dilution has remained the simplest and fastest.

A major challenge of using erythrocytes as fluorescent dye carriers is how to entrap the cargo without compromising the erythrocyte integrity. For the electroporation procedure, a number of parameter were studied. The temperature prior to electroporation was lowered to 0-4°C, aiming to expand the lifetime of the transient pores formed. The erythrocytes were re-suspended in a formulated electroporation buffer during the procedure with the intent of improving efficiency and minimizing erythrocyte cellular modification. Post electroporation erythrocytes resealing, temperature and incubation parameters were investigated for recovery. For the hypotonic dilution procedure, looking to increase loading efficiency and generate uniformly loaded erythrocytes, mixing throughout the procedure and an extra centrifugation step to concentrate the loaded erythrosensors were studied. The extent of the limitations associated with these procedures include low encapsulation efficiency, non-uniform dye loading and loss of hemoglobin, which affects intrinsic cellular functions [13,40,62,84].

Bovine erythrocytes were used in lieu of human erythrocytes. Erythrocytes were loaded using established protocols for both procedures. Smaller than human erythrocytes,

bovine erythrocytes have a diameter of 5 μm. In addition, human and bovine erythrocytes have different membrane phospholipids and protein arrangement. Zimmerman et al. (1982), showed data indicating that, although bovine erythrocytes are smaller, a higher field strength electroporation is required, compared to human erythrocytes electroporation response [85,86]. It has also been reported that, although after electroporation the pore size doesn't seem different, the leak permeability, defined as the measurement of tracer fluxes, differs. At 0°C the pores are stable and increasing the temperature rapidly reseals the membrane [75,87,88]. Another important difference between human and bovine erythrocytes, is that the bovine erythrocyte lifespan is around 160 days.

Confocal microscopy has been used to study the distribution of FITC-labeled BSA, and other molecules within carrier erythrocytes in drug delivery [84]. However, little is known about the cargo location, external or internal. In this study, we compare the fluorescence of loaded erythrocytes with that of "empty" carrier erythrocytes and control erythrocytes. To verify volume-loading capacity, z-stack confocal images were analyzed. To explore species independence, both rat and bovine erythrocytes were evaluated for loading uniformity, and morphology.

Using AFM, the topography and shape of carrier erythrocytes was studied. AFM allowed semi-destructive imaging since the cells were fixed. High-resolution topography reveals details at the subcellular level. Furthermore, different AFM modes can be used to control the nano-stimulation and investigate the physiological properties of erythrocytes.

To understand the morphological changes in erythrocytes loaded using the hypotonic dilution technique, AFM was used to evaluate the topography of the resulting erythrosensors.

Results

The electroporation and hypotonic dilution parameters were optimized, but first the FITC-glygly conjugation reaction was evaluated via HPLC to ensure the correct stoichiometry. A molar ratio FITC to glycylglycine of 1:4 at pH 8.0-9.0 was found to provide the highest ratio relative peak heights between unreacted FITC and conjugation product (Figure 2). Different molar ratios of FITC to glycylglycine were evaluated: the 4:1 ratio was found to have a peak height ratio of 1:20, the 1:1 ration was found to have a peak height ratio of 1:2 and the 1:4 ratio was found to have a 37:4 peak height ratio. Thus, showing that the FITC to glycylglycine reaction at a molar ratio of 1:4, reveal a higher peak height ratio indicative of increased conjugation of FITC-glygly and less unreactive reactants.

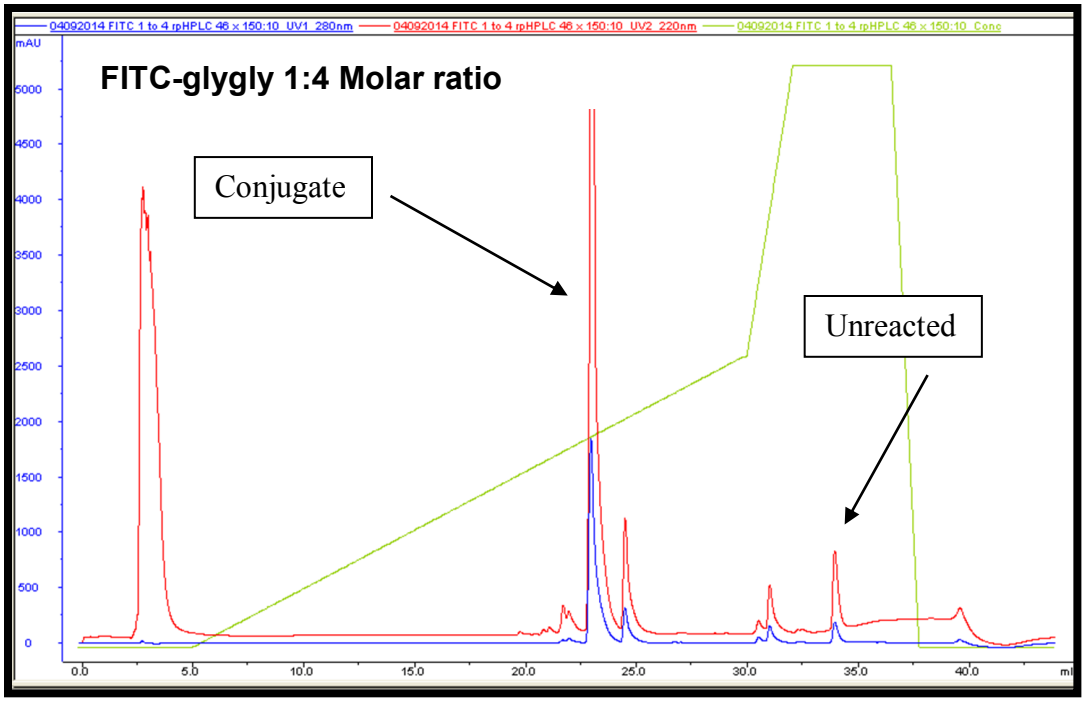

Figure 2. FITC-glygly conjugation verified by HPLC. A reference standard solution was used for reactant FITC identification. FITC-glygly at a molar ratio 1:4 had the highest peak height ratio.

To investigate the conditions for FITC-glygly erythrocyte loading via electroporation, the voltage amplitude effect on the erythrocyte diameter size were compared. Then the fluorescent signal at different amplitudes was evaluated. Electroporation was performed at various amplitudes to optimize cell survival and loading. The effects of electroporation at different amplitudes on the diameter of the carrier erythrocyte were assessed and compared with the diameter findings of the native erythrocytes. In addition, the fluorescence per cell was evaluated as a measurement of loading efficiency at the respective amplitude.

As an initial assessment, the size of the erythrosensors generated via the electroporation procedure were compared with control erythrocytes. Normal bovine erythrocyte diameter measure 5.5 - 5.8 μm in diameter [89,90]. The control erythrocytes were found to have a diameter mean of 4.896 μm +/- 0.297 standard deviation, which lies below the normal erythrocyte diameter. Erythrosensors diameter electroporated at 200 V and 300 V, exhibit not significant, ns ($p > 0.05$) difference to the erythrocytes diameter of the control cells. A slightly smaller average diameter for the cells (except by cell electroporated at 750 V or more) was retained (Figure 3). The cell size of the control cells and experimental samples was found to be around 5 μm. When compared to the control cells, the bright field images reveal similar size. Cells electroporated at 200 V were found to have an average size of 4.37 μm, cell electroporated at 300 V had an average size of 5.32 μm, and cells electroporated at 750 V had an average size of 5.73 μm. Cells electroporated at 750 V had the largest diameter size, and also the greatest variation between size, which can account for erythrocytes swollen, lysed, and debris fragments.

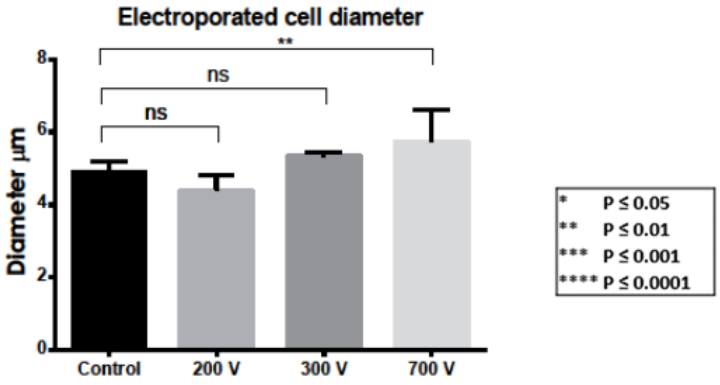

Figure 3. Average erythrocyte size for electroporated cells at different amplitudes. Error bar represent the standard deviation. The symbol ns indicates p >0.05.

As shown in fluorescence micrographs and corrected total cell florescence chart, samples electroporated at 300 V seem to have significantly more FITC-glygly fluorescence per cell than the other samples (Figure 4). Overall, electroporated erythrocytes had the most fluorescence per cell at 300 V amplitude and 1 ms pulse width. At 200 V at 1 ms, it was found that the cells had approximately half the fluorescence per cell as the erythrocytes electroporated at 300 V. Cells electroporated at 200 V most likely did not load as well because the size of the pore is dependent on the amplitude applied.

The average corrected total cell fluorescence (CTCF) at 300 volts was found to be the highest among the samples evaluated. For the 300 V electroporated erythrocytes CTCF the outlier fluorescence on the image was omitted from the data (Figure 4). This outlier is most likely a FITC-glygly aggregate. Control erythrocytes exhibit no florescence as

expected, indicating no auto fluorescence associated with cells. Erythrocyte electroporated at 200 V and 1 ms pulse width exhibit lower fluorescence per cell than the erythrocytes loaded using amplitude of 300 V and the same pulse width. The samples electroporated at 750 V had the least fluorescence detected, probably due to the irreversible break down of cells, lead to complete hemolysis and a mix of FITC-glygly and erythrocyte debris.

Electrical hemolysis of bovine erythrocytes was also observed. The resulting micrographs show erythrocyte lysis/death at 750 V. The cells electroporated at 750 V and above exhibited increased cell death and debris as amplitude increased (data shown for 750 V only). At 750 V, cell rupture due to the irreversible breakdown is shown. Cell debris, and fewer cells are observed in the micrographs. This indicates that threshold value of the electric field was at or above what Erythrocyte membrane could withstand.

The characteristic morphology of erythrocytes is not evident from the micrographs. Only the circular outline is seen in the micrographs. The control and the 300 V electroporated erythrocytes have the distinct ring shaped contour. However, the contour of the cells electroporated at 200 V is obscured by the brightness of the image. At 750 V, there are only sporadic cell outlines discernible, with irregular contours.

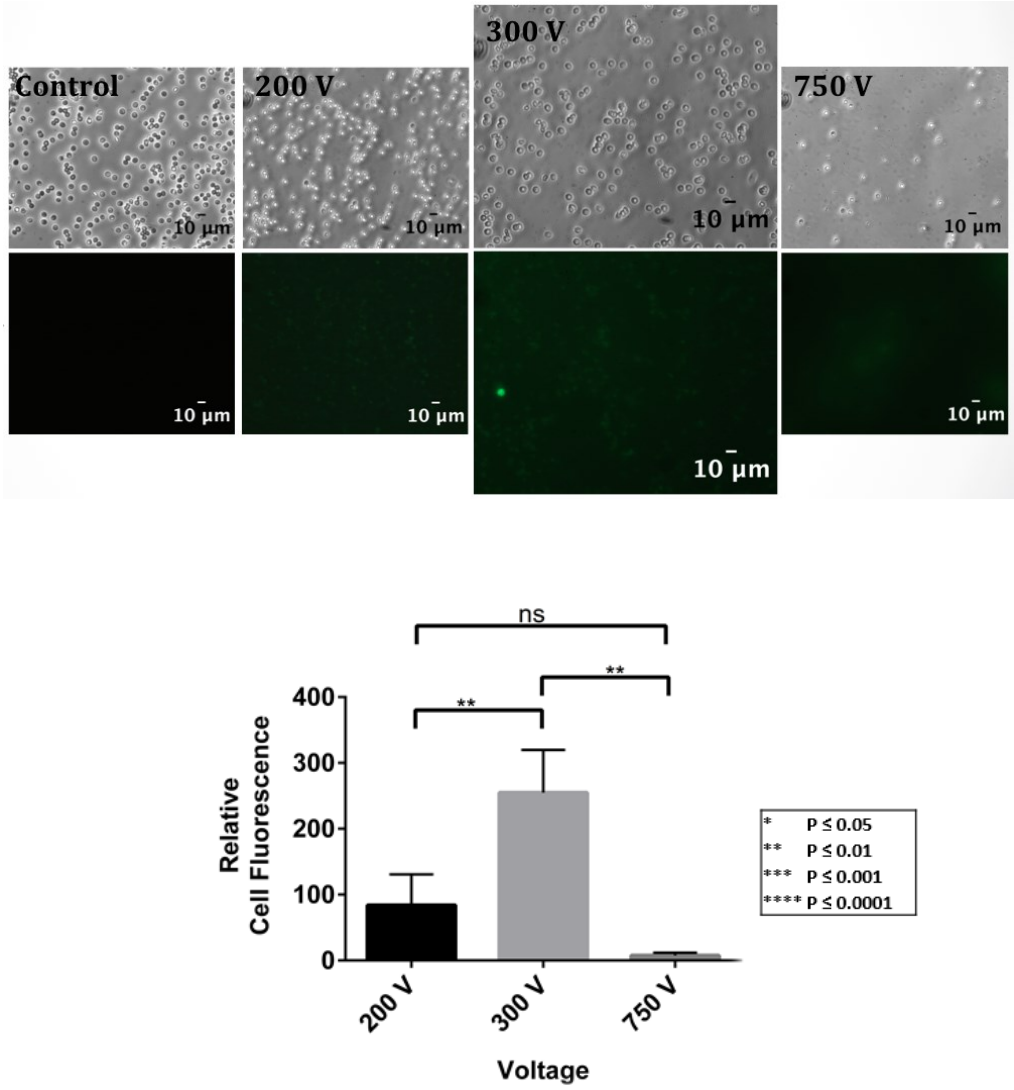

Figure 4. Erythrocytes electroporated at different amplitudes. Top: Fluorescent micrograph. Bottom: Relative cell fluorescent at different amplitudes. The symbol ns indicates p >0.05.

The absorbance curve for hemoglobin release into the supernatant shows the presence of both hemoglobin and FITC (Figure 5). Hemoglobin release was diminished with the use of electroporation buffer. Hemolysis was evident in samples electroporated

at 400 V and higher. Further analysis was done to compare with the release of cells loaded via hypotonic dilution. At 200 V and 300 V there was a similar curve (shown below). The hemoglobin sample correspond to the normal release of a control erythrocyte sample at 4°C. Absorbance curves of supernatant after electroporation revealed a FITC related peak at 492 nm and hemoglobin related peaks at 540 nm and 575 nm.

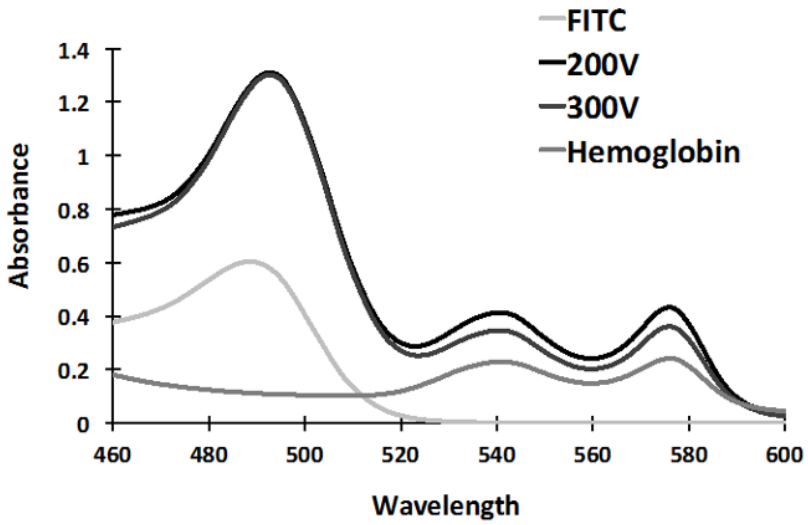

Figure 5. Electroporation: Absorbance curve of hemoglobin released in supernatant. Spectra curve of supernatant showing hemoglobin released from naive erythrocytes (hemoglobin), FITC-glygly (FITC) and carrier erythrocytes loaded by electroporation at two different amplitudes (200 V and 300 V).

To assess the optimal pulse width, cells were stimulated at 300 V, with pulse widths of 0.5 ms, 1 ms, or 5 ms every 15 minutes through four cycles. The square wave pulse used for this experiment maintains a constant level during the length of the pulse.

Control cells were electroporated using the longest pulse time, 5 ms. Erythrocytes electroporated at 300V using a pulse width of 1 ms had a significant amount of fluorescence detected by fluorescence microscopy. Thus, varying pulse length and the constant 300V amplitude was studied to identify the ideal conditions for loading FITC-glygly into bovine erythrocytes (Figure 10).

The fluorescence of erythrocytes loaded via electroporation using different pulse widths was shown in figure 6. A trend of increasing cell fluorescence with decreasing pulse length was revealed. Control erythrocytes exhibit no auto fluorescence. Bright field micrographs show similar Erythrocyte population. The fluorescent micrographs hint that the erythrocytes which were pulsed for 0.5 ms with 300 V, showed the most fluorescent per cell. As can be seen from the corrected total cell fluorescence for this sample indeed the 0.5 ms pulse length attained the highest levels of fluorescence per cell. The erythrocytes electroporated with a pulse length of 1 ms, had lower fluorescent per cell, while the erythrocytes electroporated by 5 ms exhibit the lowest fluorescence per cell.

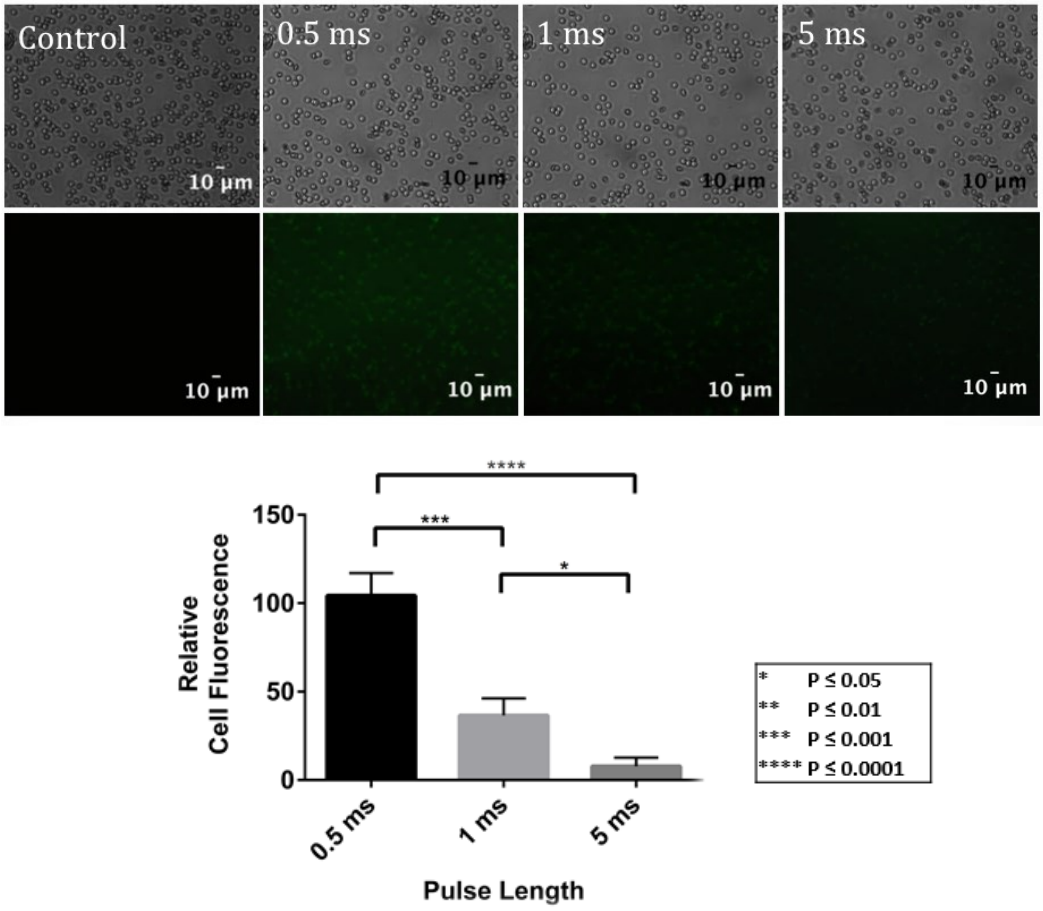

Figure 6. Bovine erythrocytes loaded via electroporation. A voltage of 300V and different pulse widths were used. Bright field images (top) and fluorescent micrograph (bottom) are shown. The fluorescent per cell revealed at different pulse widths.

Turning to the experimental evidence on loading erythrocytes using the hypotonic dilution method. Figure 10 shows that cell loaded efficiently. To characterize the loading efficiency and visualize the loaded-RBCs, fluorescence from FITC was detected using fluorescent microscopy. Following the use of FITC-glygly at pH 9.0 and the gentle mixing

of cells every 10 minutes during the incubation at 37°C, an increase in cell loading was noted.

From the 20X fluorescent and bright field micrograph it is difficult to describe if the cells maintain their biconcave shape (Figure 10). However, the cells appear as circular erythrosensors in the bright field micrographs. By means of fluorescence microscopy, it was observed that the fluorescence of the cells seems higher than using electroporation. Photobleaching was observed after 2 seconds imaging, which could interfere with the fluorescence signal detected in our results as shown in the images below.

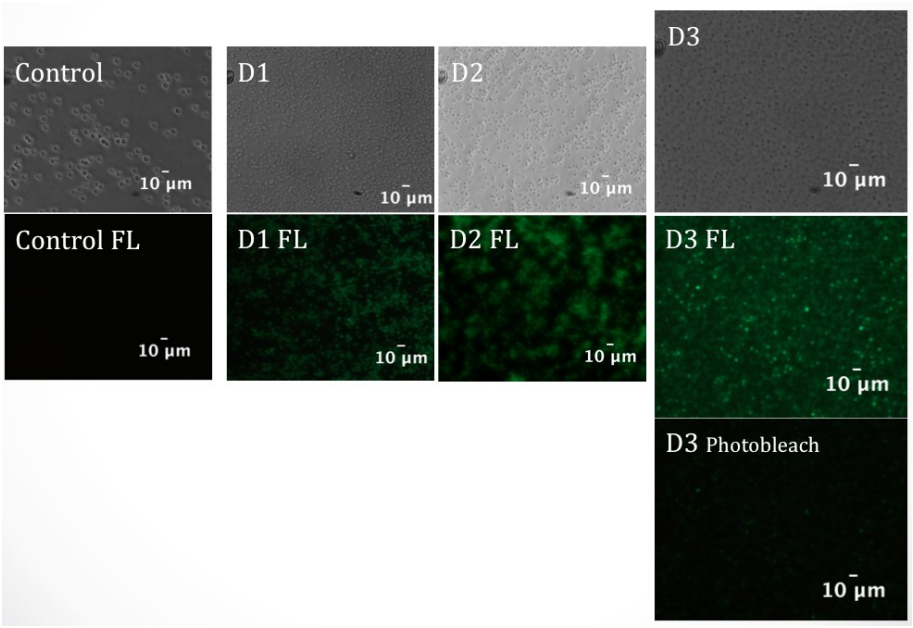

Figure 7. Erythrocyte loaded with FITC-glygly via hypotonic dilution. (Top) Bright field images of "ghost" erythrocytes and fluorescent images of three experiments D1, D2 and D3 (Middle). Right-bottom image of photo bleaching after 2 seconds exposure (D3)

The recordings of the absorbance of the supernatant on the spectrophotometer are comparable to the readings of electroporated cells (Figures 5 and 8). The absorbance measurements of the supernatant shows the presence of both hemoglobin and FITC (Figure 8). The hemoglobin sample corresponds to the normal release of a control erythrocyte sample at 4°C and the absorbance peaks are shown at 540 nm and 575 nm. Absorbance curves of supernatant after hypotonic dilution also revealed a FITC related peak at 492 nm. The absorbance spectrum corresponds to diluted samples (Hg1 and Hg2), taken from two representative experiments.

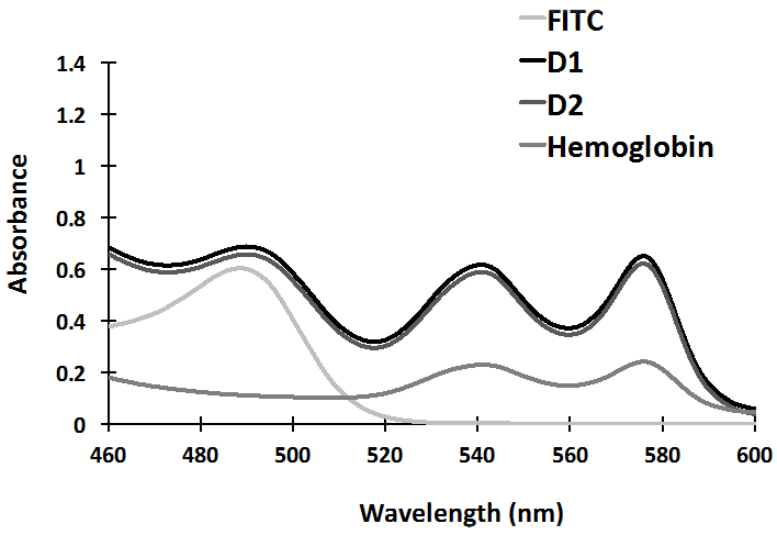

Figure 8. Hypotonic dilution: absorbance curve of hemoglobin released in supernatant. Spectra curve of supernatant showing hemoglobin released naive erythrocytes (hemoglobin), and hypotonic dilution erythrosensors (D1 and D2)

Looking at the concentration of hemoglobin inside the erythrocytes loaded via electroporation, the erythrocytes maintained significantly higher levels of hemoglobin than the cells loaded using hypotonic dilution. The three samples of different experiments, control, hypotonic dilution erythrosensors and electroporation erythrosensors, were evaluated and compared for hemoglobin content (Figure 9).

Normal bovine erythrocytes contain between 8-15 g/dL hemoglobin [39,89]. The hemoglobin in the control sample was estimated to be between 8.808 +/- 1.409 g/dL, which stands in the lower range of the normal bovine erythrocyte hemoglobin concentration. This may be due to handling and process, or spontaneous leakage of hemoglobin throughout the experiment. Overall, this is a good standard control, which correlates well with the literature.

The figure 9 shows that cells loaded using hypotonic dilution lost the most hemoglobin through the loading process. The concentration of hemoglobin inside the erythrosensors loaded using hypotonic dilution was found to be in the range of 1.004 +/- 0.559 g/dL. This is in accordance with the results showing a significant amount of hemoglobin in the supernatant after loading. The cells lost approximately 89% of their initial hemoglobin content. Losing this much hemoglobin will be a challenge for the survival of erythrosensors produced using the hypotonic dilution technique. The average hemoglobin concentration inside cell loaded via electroporation was approximately 5.632 +/- 0.589 g/dL. On average, electroporated erythrocytes lost approximately 46% of the

total hemoglobin. As shown in figure 9, erythrosensors created using electroporation retained higher concentrations of hemoglobin.

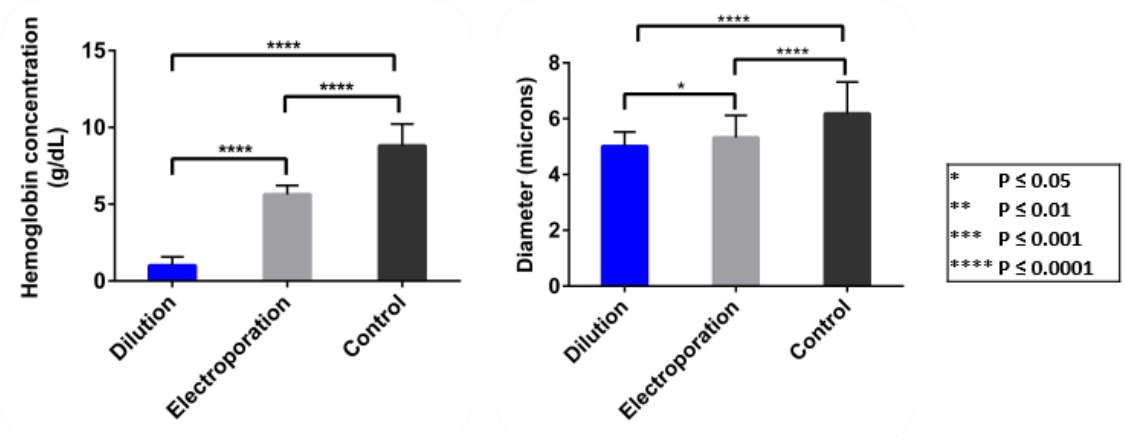

Figure 9. Diameter, and hemoglobin content of erythrosensors. Absorbance at 540nm of lyse control erythrocytes and erythrosensors prepared using the hypotonic dilution and electroporation procedure.

The CTCF was used as a measurement of fluorescence intensity per cell in the sample (Figure 10). The average CTCF of the cells in the micrograph was calculated using Image J software to segment 4 images per condition. A total number between 100-150 cells were evaluated for each procedure. The results of erythrocytes loaded via hypotonic dilution were compared to those of cells loaded using electroporation. The difference in cell fluorescence intensity between samples was evident from the micrographs. This quantification was applied to uniform samples; ten randomly chosen cells for each micrograph were evaluated. The results revealed that cells loaded through

hypotonic dilution, had four times more fluorescence intensity than cells loaded using electroporation.

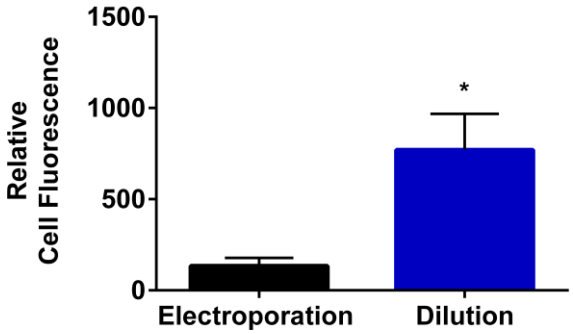

Figure 10. Cell fluorescence as a measure of loading efficiency. Corrected total cell fluorescence of ten randomly chosen cells from a 20X micrograph representative of cell loaded by electroporation or hypotonic dilution. Cell's integrated density, Area and the mean fluorescence of the background were used to evaluate the average fluorescence signal per cell. * $P \leq 0.05$

Confocal microscopy and AFM were used to evaluate key cellular features in the erythrosensors. Confocal fluorescent micrographs show different loading levels among a sample and further processing was established to concentrate cells with similar loading efficiency. AFM revealed changes in the topography, and stability of the cell and its membrane. In addition, both procedures were used to evaluate the size and morphology of erythrosensors. The resulting images show strong evidence that erythrosensors loaded via hypotonic dilution are damaged; this could impact erythrosensors *in vivo* lifespan.

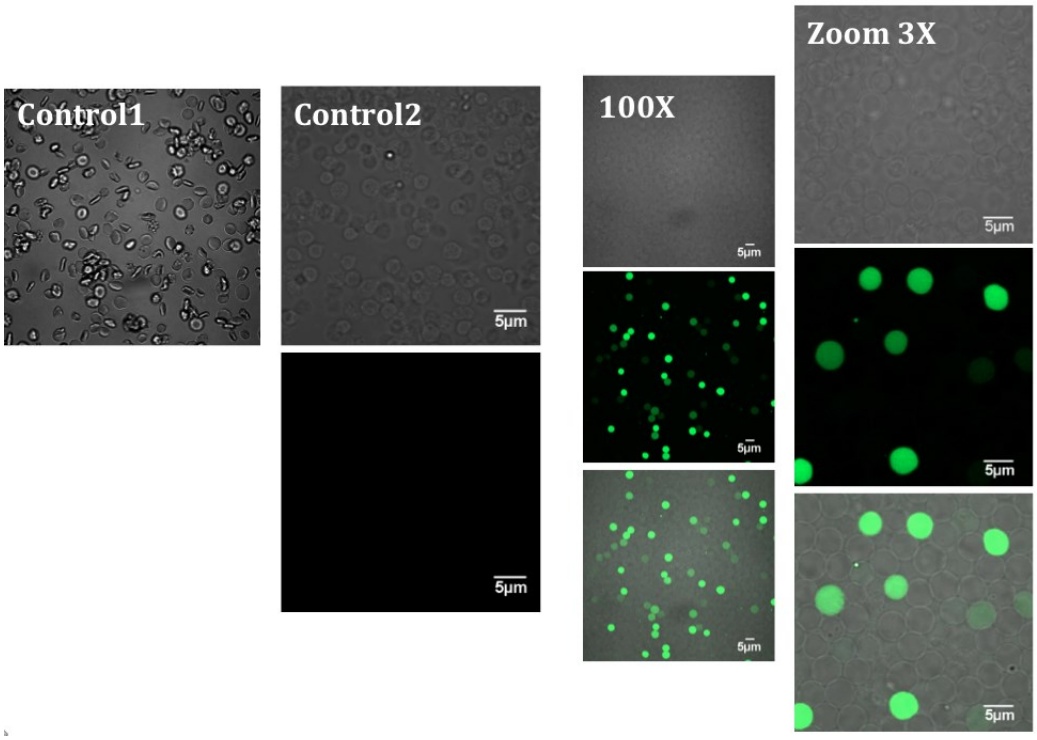

Figure 11. Confocal micrographs of control carrier erythrocytes and erythrosensors. Control1: native erythrocytes. Control2: Auto fluorescence control, erythrocytes were subject to hypotonic dilution without FITC-glygly.

Confocal micrographs obtained from two controls and a sample of bovine erythrocytes loaded via hypotonic dilution provides a close look at the different erythrosensor formation and the mixed loading efficiency (Figure 11). The control1 show native erythrocytes which were subjected to the same temperature and centrifugation condition as the experimental samples. The control1 erythrocytes exhibit the distinctive shape of normal erythrocytes. To show that the fluorescence detected is associated with loading of FITC-glygly and not an artifact of auto fluorescence, the second column of micrographs shown in figure 11, presents images from native erythrocytes loaded via

hypotonic dilution with no FITC-glygly and resulting in membranes without fluorescence (control2). The dilution process to load FITC-glygly on experimental samples was carried out as before; the samples showed a non-uniform dye loaded population of erythrocytes with approximately 30% exhibiting fluorescence, while different erythrosensors in the micrograph exhibit varying levels of fluorescence.

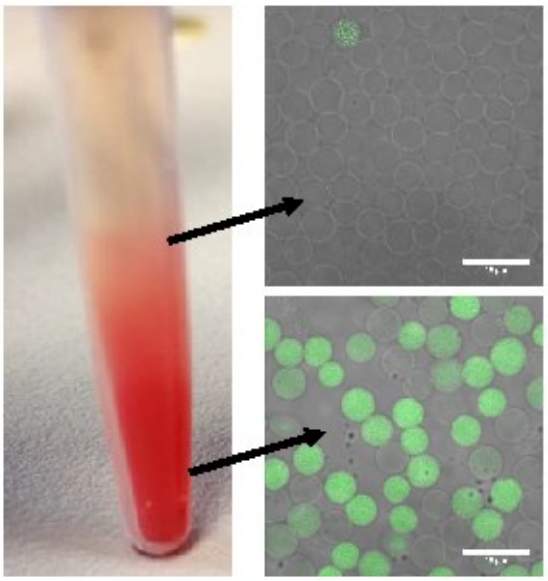

Figure 12. Separation of cargo loaded erythrosensors. Cell were separated by centrifugation.

The results obtained from the preliminary analysis of confocal images of erythrosensors loaded via hypotonic dilution, are shown in Figure 12. It is apparent that fully loaded cells are diluted within unloaded cells. To concentrate loaded and unloaded cells by density, centrifugation for 5 minutes at 10000 g was used. The samples layers

were imaged, revealing highly loaded cells at the bottom (Figure 12). For standardizing the methods to evaluate fully loaded erythrosensors, this centrifugation process was used for the remaining of the experiments.

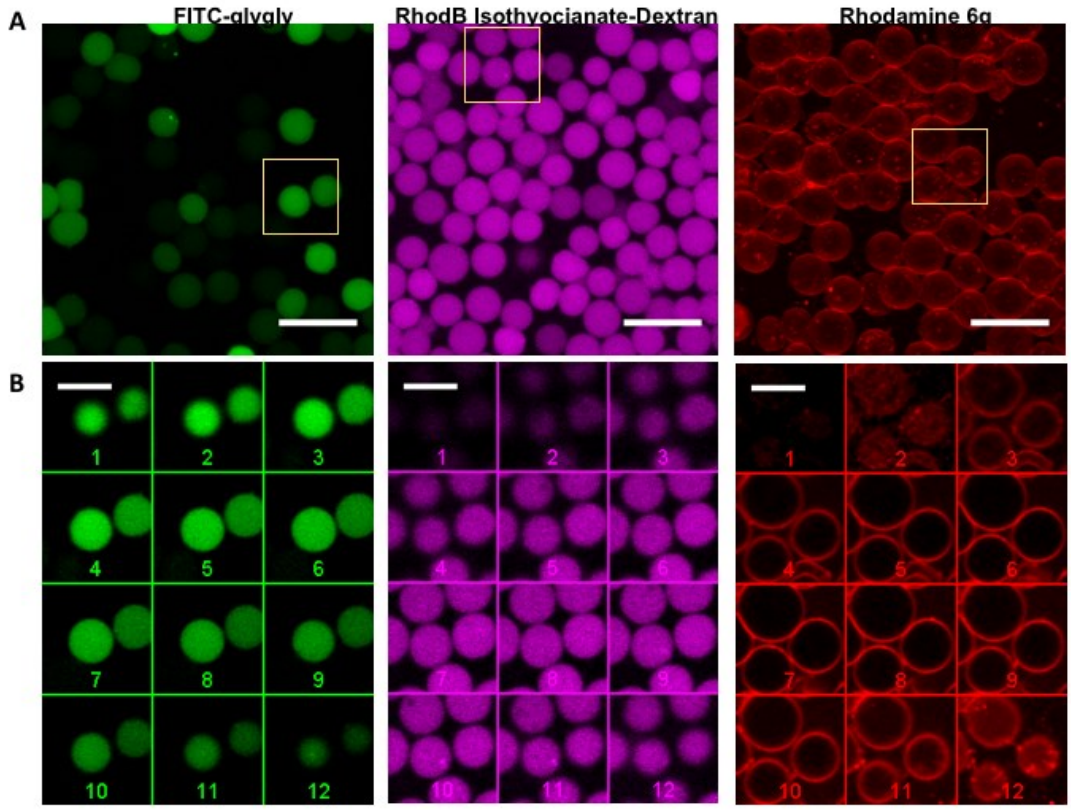

Figure 13. Z-Stack of erythrosensors entrapping different cargo. FITC-glygly, TRITC and Rhodamine 6G were used. A. Representative maximum intensity projection for each cargo. B. z-stack with step size between images shown is 45 µm.

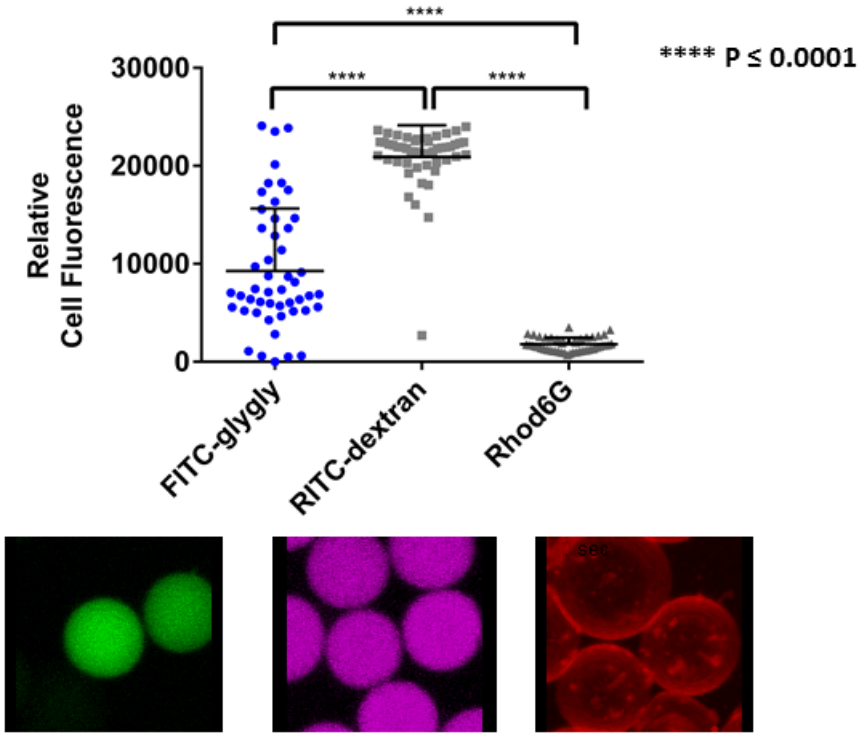

Figure 14. Loading different dyes using hypotonic dilution. Analysis of dye internalization shows the standard deviation differences and mean value. FITC-glygly exhibit more variance on the loading, while RITC-dextran (commercial dye) load more homogeneously through all the erythrosensors. Rhodamine 6G, show not internalization at all.

Z-stack micrographs of erythrosensors revealed non-uniform FITC-glygly loading within the erythrosensor (Figure 13 and Figure 14). Fluorescent images show the fluorescence of FITC-glygly through the erythrosensors. So far FITC-glygly has been used to study erythrosensors, a question about if the loading efficiency was perhaps fluorescent dye dependent emerged. The fluorescent dye chemistry could play an important role throughout the loading procedure. To compare the loading entrapment efficiency, the same hypotonic dilution procedure using different dyes was performed. A dextran labeled

with rhodamine B isothiocyanate (TRITC), used in drug delivery studies and a lipophilic probe commonly used to study membrane transport were evaluated. The cell recovery calculated as the ratio of the resulting erythrosensors packed volume to the initial packed erythrocytes volume, remained the same for the three dyes, around 10%. After isolation, 80% of erythrosensors loaded via hypotonic dilution using FITC-glygly had some entrapment, compare to >98% when using TRITC. As expected Rhodamine 6G seems to associate with the cell membrane thus leaving a hollow non-fluorescent space inside the cell, demonstrating the fluorescent membrane (outline) of the erythrosensors and showing the least entrapment.

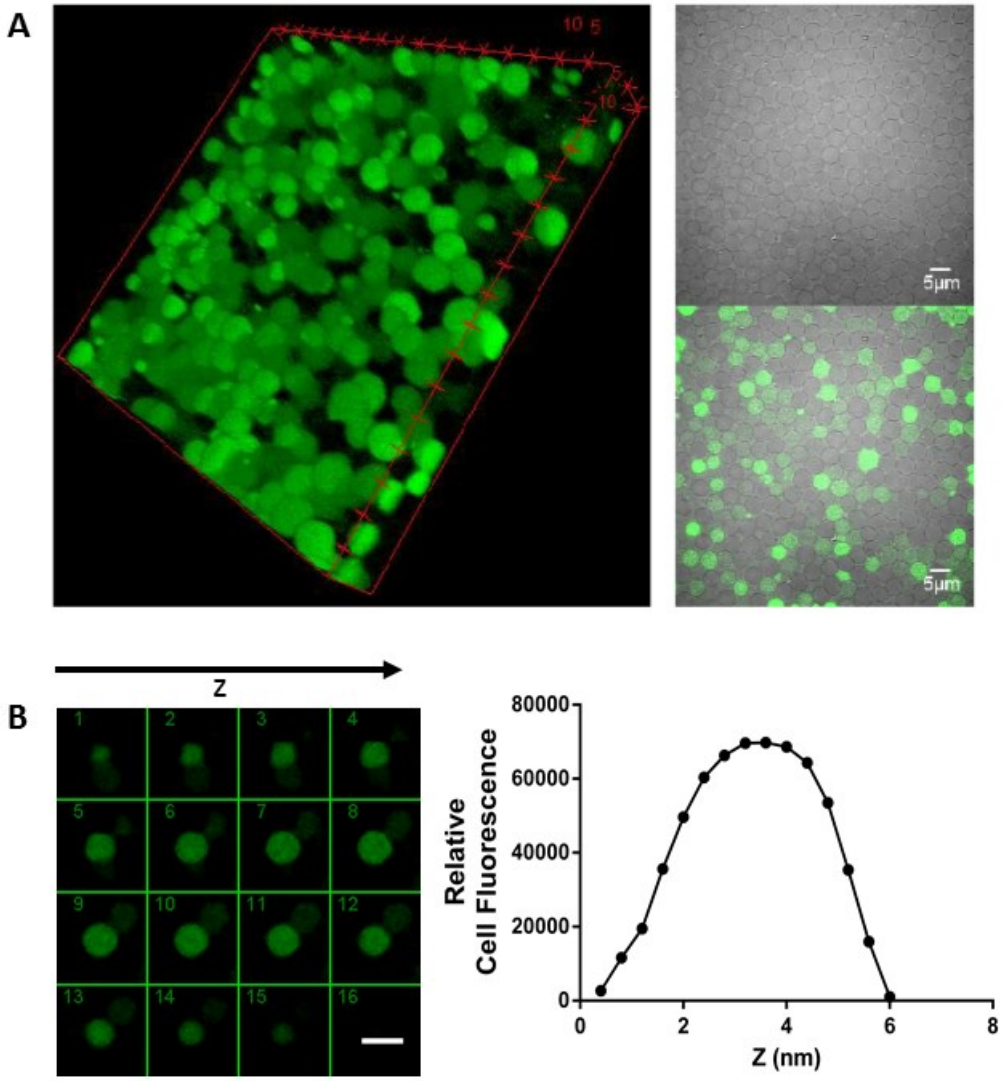

Figure 15. Volume rendering sequence of FITC-glygly loaded erythrosensors. A. 3D-image of FITC-glygly loaded bovine erythrocytes showing their spherical shape as the image is rotated on the x-axis. On the right a micrograph shows a single section of the z-stack. B Cropped z-stack of single erythrosensor sequential slice 1 through 16 with a 0.40 µm step. On the right the relative cell fluorescence at each step.

A representative movie of a Z-stack created using a step size of 0.40 µm to evaluate the loading uniformity of the population and of the FITC-glygly entrapment (Figure 15). Figure 15, presents the first image of the z-stack on the right, the sequential images were process to create the volumetric image and then rotated 90 degrees over the x-axis to reveal the distribution of FITC-glygly within the vesicle. It can be seen from the relative cell fluorescence graph that the erythrosensors are volume loaded, and the FITC-glygly is not just associated with the membrane. In fact, fluorescence is detected throughout the erythrosensors and shows that FITC-glygly is encapsulated within the erythrosensors. Interestingly, the 3D reconstruction animation of the z-stack fluorescent micrographs also revealed a spherical shape.

Rat and bovine micrographs in figure 16show both types of erythrosensors loaded with FITC-glygly and their disk-like shape. Rat erythrosensors seem to entrap FITC-glygly more uniformly than bovine according to the micrographs (Figure 16a). When the optical signal was evaluated, it was found that the rat erythrosensors had twice as much signal than bovine erythrosensors (Figure 16b). Rat and Bovine erythrosensors images were taken at different sections of the slide. This minimizes the possibility that the attenuation of the signal in bovine erythrosensors may be because FITC photo bleaches quickly.

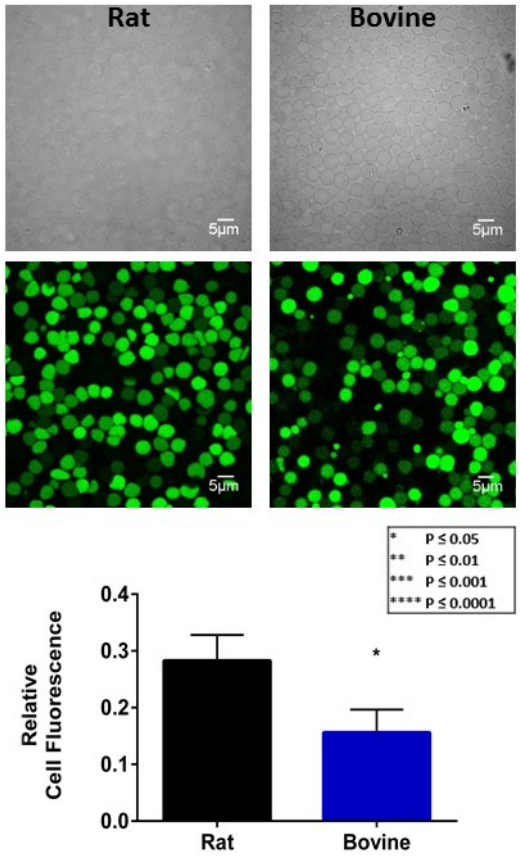

Figure 16. Rat and bovine erythrosensors. Top confocal images comparing rat and bovine cells loaded via hypotonic dilution. Bottom relative cell fluorescence for each samples.

The results obtained from the preliminary analysis of the erythrosensors morphology via confocal microscopy, showed a spherical shape (Figure 17). To further understand the changes in morphology, AFM was used to study the topography and the cross-section profile. The findings were compared with the resulting data collected from native erythrocytes as controls.

AFM results show a 40 µm x 40 µm scanning area and its corresponding topographical image (Figure 17). Control erythrocytes exhibit their characteristic shape and dimensions: disc shape with a 5-6 µm diameter and 1-2 µm heights, in accordance with normal diameter and height of erythrocytes in literature. The topographical image revealed the surface profile of erythrocytes (Figure 17). This 3D image shows the different stages of erythrocyte deformation. From this image, the biconcave morphology of normal native erythrocytes as well as erythrocytes with abnormal shapes (acanthocytes - spheroids and echinocytes - burr cells) can be observed. In a blood sample, it is normal to find such a population with cells at different stages of their life cycle. The abnormal erythrocytes found in this sample may be part of the aging population of erythrocytes in the sample, an artifact created by mishandling of the sample or by the test itself.

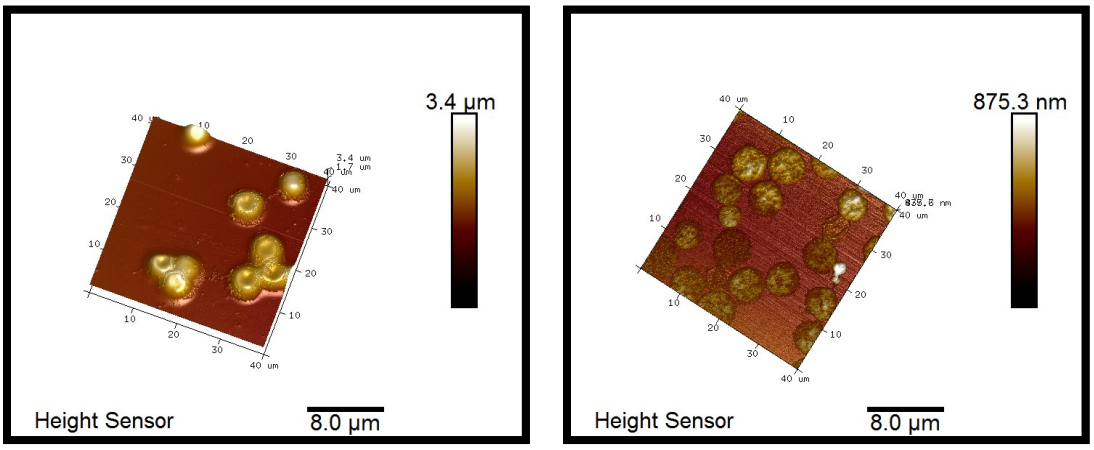

Figure 17. AFM topographical profile of normal erythrocytes and erythrosensors Profile of normal erythrocytes (left) and erythrosensors (right).

The erythrosensors imaged on Figure 17 reveals major morphological changes. The highest peak detected is on the erythrosensors topography is 875 nm. This peak does not account for the multiple valley, and irregular surface seen throughout the sample. Erythrosensors average diameter was irregular when compare to the normal diameter of native erythrocytes; the shape is circular, but flattened and only one third of the average height of a normal bovine erythrocyte (Figure 18-20). Figure 17 shows an example of the differing sizes and shapes found in a sample of erythrosensors. The average diameter for erythrosensors was found to be 4.48 µm, and the average height was 798.36 nm +/- 421.243 standard deviation. This height average is about one half of the normal height for a native erythrocyte. However multiple hills and valleys are appreciated in the topographical images.

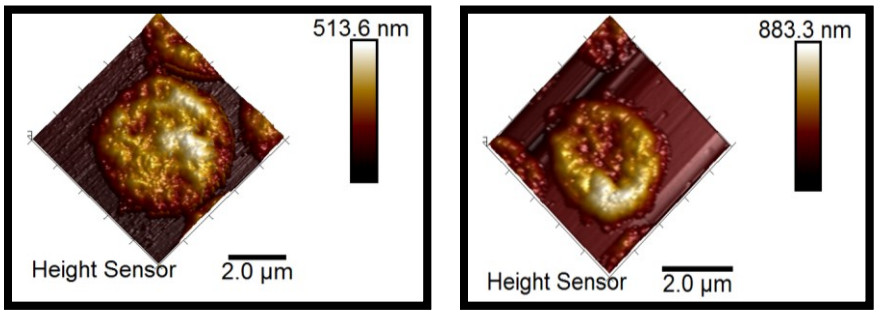

Figure 18. Erythrosensors topography reveals hills and valleys in their surface. The heights of the erythrosensors shown in this images lies between 513-883 nm

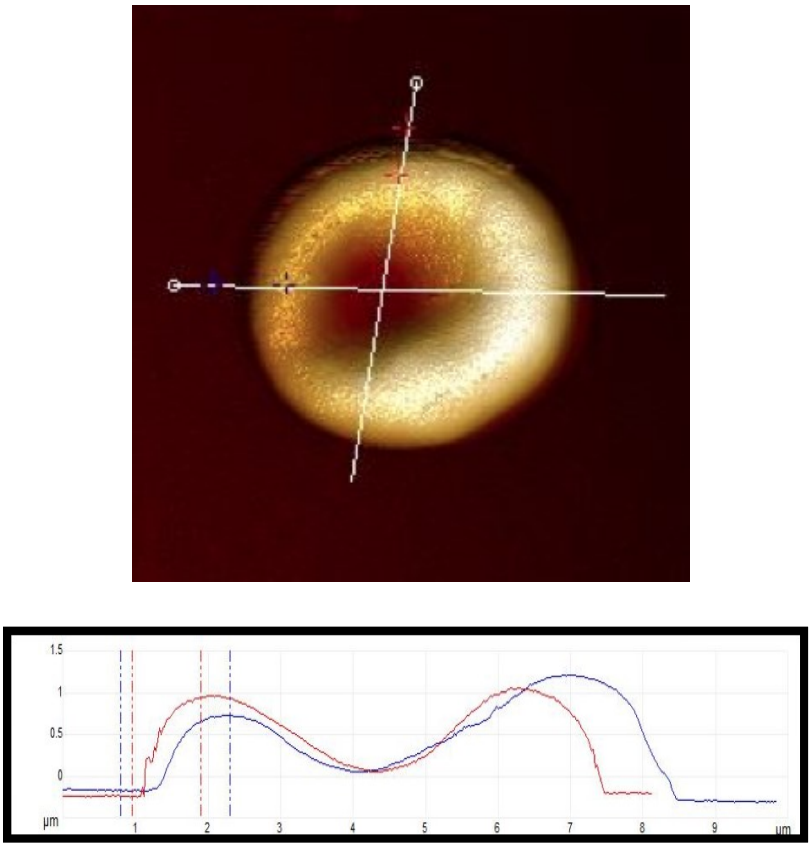

Figure 19. Cross-section profile of normal bovine erythrocytes

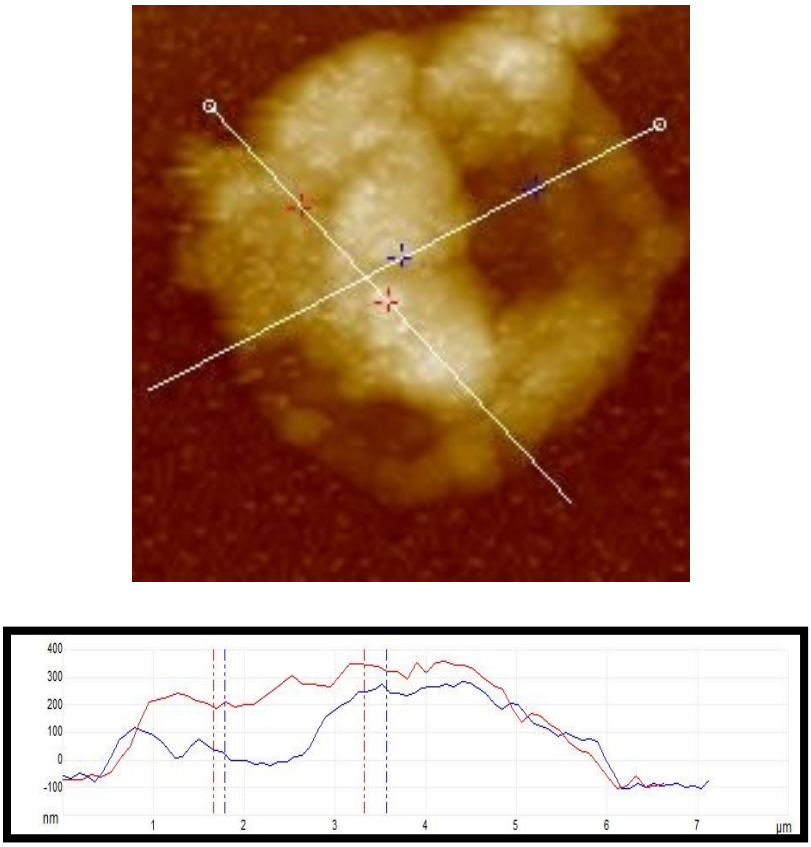

Figure 20. Cross-section profile of erythrosensors.

The roughness of the topography of the control erythrocytes and the erythrosensors exhibit differences in the topographical images, and upon quantification, the Ra value, which measure the deviation from the mean line and calculated using Bruker NanoScope analysis software. The Ra value was found to be greater in erythrosensors (Figure 21). The control erythrocytes have a normalized Ra value at 0.14 nm, while the Ra value for erythrosensors could be twice as the Ra value for control cells. In addition, the Ra value was found to be more variant for erythrosensors.

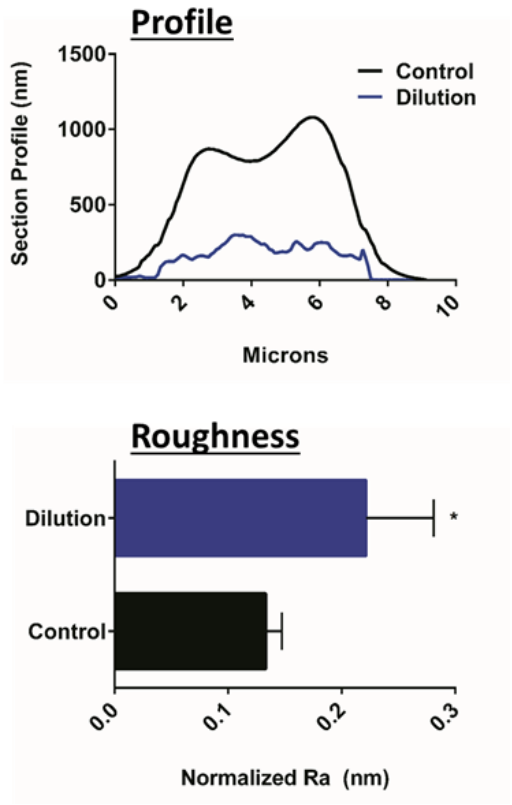

Figure 21. Ra value, measuring roughness of the surface. The mean of the absolute vertical deviation from mean line of the topographical profile. * P > 0.05

Discussion

Erythrocytes loaded via hypotonic dilution and electroporation maintained the disc shape needed to engineer successful erythrosensors. Abnormal shapes usually occur because of problems with the cytoskeleton or membrane, or secondary reasons including precipitation of hemoglobin. The cell flexibility is also dependent of the cell membrane, and the cytoskeleton. Factors affecting the yield, integrity and the performance of carrier erythrocytes include: improper handling of cells, susceptibility to hemolysis, bio

distribution, *in vivo* stability and blood-borne diseases. Still, the *ex-vivo* artifacts of engineered carrier erythrocytes are not well understood and further optimization is required to minimize structural alterations and increase lifetime circulation.

Loading erythrocytes using the hypotonic dilution method seems to achieve a more uniform/higher loading than loading erythrocytes with the same concentration of fluorescent dye using the electroporation method. Analysis of the absorbance at 540 nm, as a measurement of hemoglobin release, shows that the hypotonic dilution method causes the erythrocytes to lose more hemoglobin than the electroporation method. This study addressed the need to further understand and quantify changes to the erythrosensors by the process of encapsulation.

It is imperative for the field, and necessary for the project, to evaluate efficiency of different protocols for loading erythrocytes. In addition, developing methods in accordance to with our aims (i.e. maintain intrinsic cell functions) is essential for the survival of the erythrosensors *in-vivo* and their sensing ability [11]. Our findings lay the basis for the characterization of encapsulation yields for Erythrocyte-based sensing.

This study strived to further study changes in erythrosensors characteristics and to develop protocols for the characterization of the physical properties of erythrosensors. Cellular changes jeopardize the erythrosensors ability to circulate through poorly accessible capillaries. Characterization of erythrosensors loaded using the hypotonic

dilution included the evaluation of cell size, loading uniformity and morphology. Protocols to study the loading uniformity via confocal microscopy, and the cell morphology and topography using AFM were devised. Neither carrier erythrocytes nor erythrosensors' cellular properties were well understood. Therefore, this study was step toward understanding the cellular properties of erythrosensors.

The first question in this study sought to determine was the distribution of FITC-glygly within the erythrosensors. The results of this study showed that auto fluorescence was not related with the vesicles resulting from hypotonic dilution. One of the attributes of the erythrosensors loaded via hypotonic dilution is the emission of a strong fluorescent signal, which motivated the in-depth study of this loading technique. Different levels of fluorescence were detected from the erythrosensor population via hypotonic dilution, which suggests the need to further concentrate the loaded cells from the unloaded cells in the sample. Density separation by centrifugation was set as a standard for the study of erythrosensors via confocal microscopy and AFM. The resulting sample exhibits a concentration of erythrosensors with similar fluorescence. Although unloaded cells are also present in the sample. Concentrating erythrosensors with similar fluorescence increases the chances that, for example during AFM topographical images, the erythrosensors studied will be loaded with FITC-glygly. Another important finding was that loaded erythrosensors entrap the FITC-glygly within the vesicles instead of on the membrane. Before this study, the location of the fluorescence in carrier erythrocytes was not well characterized. Although past studies suggested encapsulation of FITC-glygly,

there was not actually evidence of entrapment, until now. In addition to providing the volume within the erythrosensors where fluorescence is found, z-stack confocal micrographs also support the AFM results in terms of changes to the morphology.

In the current study, the effect of the loading process on the Erythrocyte physical properties was assessed. Using AFM, the morphology, surface roughness and cross-section profiles were evaluated. Decreased size, increased deformations, and rugged topography were some of the erythrosensor attributes found here. This study was unable to demonstrate erythrosensor mechanical changes because of the need to stabilize the vesicles via fixation. Bhraler et al. also found that carrier erythrocytes had a rugged cross-section profile. The results presented in this thesis are consistent with Brahler et al. findings in which the cellular changes of carrier erythrocytes were first studied via AFM [66]. In addition, the surface roughness of erythrosensors, as measured by the Ra value (0.22 nm), is rougher than the surface of native erythrocytes (0.14 nm). The study serves as motivation and a guide to continue the comparative investigation of the properties of erythrocytes and erythrosensors.

CHAPTER IV

PRESWELLING ERYTHROSENSORS

Extreme changes in osmotic conditions cause erythrocytes to hemolyse. It is well understood that pores form in the cell membrane as it equilibrates with the extracellular environment. This rearrangement of the cell membrane permits the entrance of exogenous molecules and hemoglobin efflux. Taking advantage of this reversible response, carrier erythrocytes have been studied to advance fundamental cell biology understanding, drug delivery and targeting, imaging enhancement and recently for biosensing applications.

Senescent erythrocytes are cleared by organs of the reticuloendothelial system (RES). The loss of erythrocyte surface area leads to spherocytosis and subsequently to spleen entrapment [91] Previous studies of carrier erythrocytes have not dealt with their morphology and the role in their lifespan. In general, morphological changes lead to clearance signaling [92].

Fluorescence-based assays used to study cell biological interactions, provide a measurement of features and/or activity. Erythrosensors could capitalize on erythrocytes' cargo protection, and the navigation routes throughout the body, but as demonstrated in Chapter II the nature of the carrier erythrocytes (loaded with cargo) morphology remains unclear.

Ritter et al. studied a population of "ghost" erythrocytes non-uniformly-loaded with the pH-sensitive fluorescent dye FITC-glygly. The hypotonic dilution procedure was used. The findings included a population comprised 50-60% FITC-glygly-loaded resealed "ghost" erythrocytes and an entrapment (loading) efficiency ranging between 30-80% [13]. Moreover, loaded-erythrocytes tracked changes in extracellular pH. One issue was the resulting non-uniformly-loaded population of erythrosensors. In addition, erythrosensors must maintain physiological characteristics, and be compatible with near infrared dyes for *in-vivo* biosensing.

The major drawback of the hypotonic dilution procedure include the considerable loss of hemoglobin (Figure 9) [85,93-95]. Ritter et. al. work required low hemoglobin erythrocyte carriers because FITC optical properties (excitation and broad emission spectrum peak wavelengths of 495 nm/519 nm) conflicted with hemoglobin (oxy and deoxy) absorption (540 nm). It is known that hemoglobin abnormalities contribute to morphological changes that lead to clearance from circulation [96-98]. Hence why carrier erythrocytes are commonly used for RES targeting. Changes to the erythrocytes physiology causes clearance from circulation. A desirable feature for RES targeted drug delivery but a limiting factor for long-term *in vivo* biosensing.

Hypotonic preswelling is method develop by Rechsteiner which uses hypotonic conditions to drive the swelling to the lysis point [99]. It has been reported that this procedure causes minimal damage to the erythrocyte [41,100,101]. The procedure relies

on controlled swelling of the erythrocyte multiple times using a hypotonic buffered solution and an equilibration period (2-5 minutes) between each swelling step. The swelling is continued up to 150 mOsm/kg osmolality, the know point of lysis of erythrocytes. Depending on the protocol, the tonicity restoration was achieved with a NaCl or hypertonic solution for 60 mint at 40^0C. The hypotonic preswelling has been use to load a number of drugs and calcein or FITC-BSA [99,102]. The controlled hypotonic environment, and the faster procedure are reported to contribute to the carrier erythrocytes having a lifespan like that of normal erythrocytes.

Similarly, Erydel's Cell Loader™ is an instrument designed by the Magnani group at University of Urbino, Italy to load red blood cells through sequential hypotonic buffer dilutions [53,103-109]. The Cell Loader™ has achiever 35-50% cell recovery and encapsulation efficiency of 30 %. Compared to the hypotonic dilution, with the Cell Loader™ five times more cells are recovered and the efficiency stands comparable.

Loading via the hypotonic dilution procedure, erythrocytes are subjected to an abrupt osmotic pressure change to achieve lysis of the cell membrane. While hypotonic preswelling is based on control swelling of the erythrocyte to the lysis point. Along these lines, inducing a control osmotic change to gradually swell and drive pore formation is desired to maintain physiological morphology. In addition to minimizing structural changes, increasing the fluorescence signal on cell-by-cell basis, and achieving loading uniformity is also critical to the practical application of erythrosensors. These goals led to

formulation of a protocol to load carrier erythrocytes with fluorescent sensors which conserve the intrinsic characteristics of erythrocytes. To prevent biofouling, and clearance by the RES, erythrosensors must mimic naive erythrocytes.

A simpler and faster swelling-based loading procedure was developed based on the preswelling procedure and hypotonic dilution (Figure 22). This method avoids complicated tools such as those used by the Cell Loader™. The key feature of the technique is controlling the osmolality depending on the size of the cargo molecule to achieve high hemoglobin, increased erythrosensors recovery, and uniform loading. Under appropriate condition this highly controllable, adaptable and scalable procedure efficiently loads erythrocytes while maintaining the innate erythrocyte morphology. Futuristically, we aim to incorporate a glucose fluorescent sensor. We aimed to improve survivability by taking into consideration the morphology and the hemoglobin needed to maintain physiological features and function.

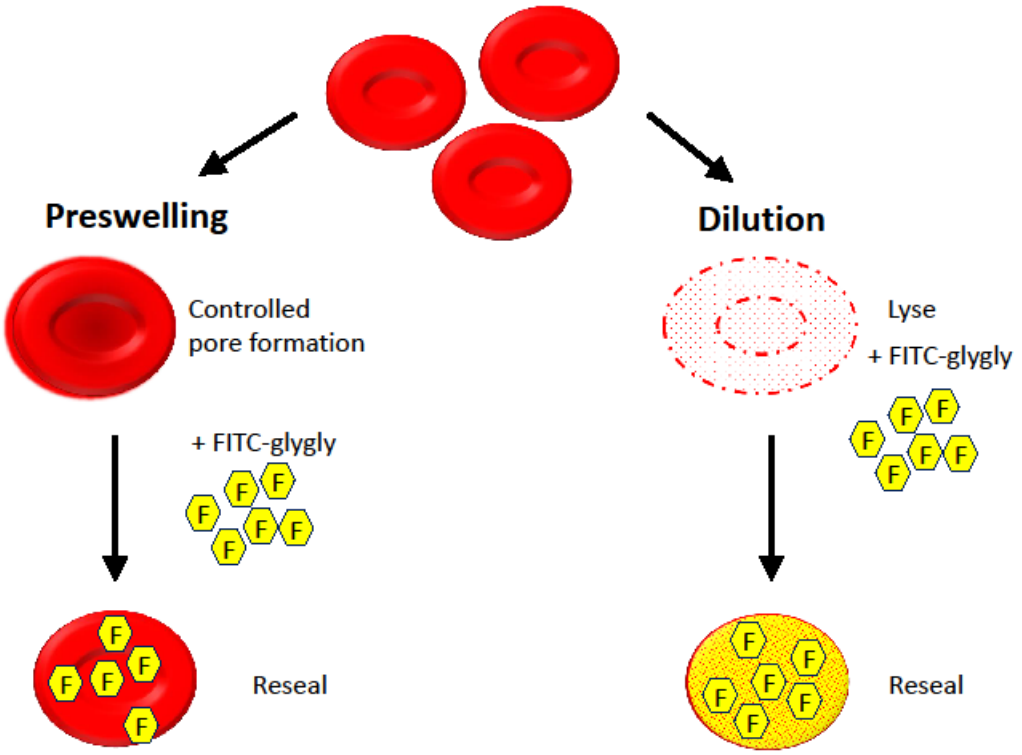

Figure 22. Preswelling vs hypotonic dilution procedure.

Erythrocytes from different species exhibit not only different surface antigens, but also differ in size, shape, and life-span. In terms of size, for example, rats' erythrocytes have an average 6.5 µm diameter human erythrocytes' diameter lies around 7.2 µm while bovine erythrocytes have a 5.8 µm diameter. Rats, bovine and human erythrocytes have a life span of 60, 160 and 120 days respectively. Erythrocytes from different species have different properties, however, the loading concept can be tailor across species. Erythrosensors derived from bovine erythrocytes were used to understand the

physiological properties, and ultimately hoping to tailor erythrosensors to specific fluorescent sensors, analytes, and targets.

Image Stream allows for simultaneous characterization of the size, shape and fluorescent signal in a per cell basis. This tool produces quantitative data of the features of a larger number of cells [92]. In this study, we characterized the percentage of recovered cells after loading, and the dimensional parameters such as the area, length. To analyze the morphology of the resulting erythrosensors, the aspect ratio and circularity were evaluated. Finally, the *in-vitro* relative level of fluorescence per cell was studied using the intensity feature.

Aiming to implement the erythrosensors into ophthalmological applications, the loading efficiency and hemoglobin levels were studied using ICG and FITC-glygly. The FDA approved dye idocyanine green (ICG) was studied for retinal imaging. ICG is routinely used in medical diagnostics particularly angiographies. It has an absorption peak at around 750-950 nm and an emission peak 810-830 nm [110,111]. The infra-red range permits deeper imaging than using fluorescein. It has a half-life of up to 180 seconds and is remove by the liver from circulation.

Results

Cells images were collected using image stream. After cell preparation, cells were washed in PBS and suspended at 50% hct. Samples were maintained in ice at 4˚C prior to

final dilution and collection. To maintain the cell morphology, cells were diluted in 1% BSA-PBS at 1:10 (V/V). Images were collected using defined parameters: 20X magnification and standard 488 nm laser at 20mW power to excite FITC. For the collection of images from the erythrocytes loaded via hypotonic dilution, 80,000-100,000 events were collected to ensure sufficient sample for analysis. A maximum of 20,000 events from triplicates for each sample were collected. The data exploration (IDEAS v.4) software package was used for analysis of the dimensional, morphological, and fluorescent features of the cell images.

Five different erythrocyte treatments were evaluated per experiment: one native, two controls (Preswelling without cargo and native erythrocytes mixed with cargo) and two experimental samples (Preswelling with cargo FITC-glygly and hypotonic dilution with cargo FITC-glygly). Native erythrocytes were used to compare size and shape, confirming that the dimensions or morphology have not change due to non-specific artefact during process and data collection. As a control to ensure that fluorescence is not due to cell auto fluorescence, erythrocytes were subjected to the preswelling treatment without any fluorescent cargo present. Native cells mixed with FITC-glygly were also evaluated to evaluate spontaneous uptake/association of the FITC-glygly with the erythrocyte membrane.

To evaluate the performance of the image flow cytometer the native erythrocytes and preswelling erythrosensors without cargo were first evaluated. The control cells

without FITC-glygly were run second, followed by the samples containing FITC-glygly in the process. Subsequently, FITC-glygly loaded erythrosensors produced via preswelling and hypotonic dilution were assessed. The erythrocytes and erythrosensors samples were suspended in 1% BSA PBS. This scheme also prevented accidental cross-contamination between samples.

Three data channels were used for the acquisition of image stream data. Channel 1 collected the calibration beads used to calibrate the instrument. Channel 5 captured a bright field image and channel 3 captured a fluorescence image. Cell classifier settings were used to collect the population of interest and ignore cell beads and debris.

To define the region of interest (mask) in the images of the gated population, two different templates were created. The first template was used for the native erythrocytes, the control and the preselling erythrosensors samples. The mask was defined using the bright field channel images and plotting the area in the x-axis and the aspect ratio in the y-axis to identify image with single cells. The second template was used for the hypotonic dilution erythrosensors. Due to low hemoglobin, the hypotonic dilution samples exhibited low contrast in the bright field channel. Thus, for the hypotonic dilution samples, the fluorescence channel was used to define the mask.

The population of single cells was defined by gating cells “face on” and “sideways” in the native erythrocytes sample and applied to both the control, preswelling

and hypotonic dilution erythrosensors. The gated region is shown in blue on figure 24. Building from the single cell population (blue gate), the images in focus were selected after analyzing the contrast and the gradient rms (root mean square of the rate of change of the image intensity profile) features. These features use the intensity variation in images to measure the sharpness of an image. Both detects large changes in pixel value but assigned different weighted values to the pixel. But, while contrast doesn't subtract the background, gradient rms does. Subsequently the dimensions of the defined population (face on and sideways) were measured using the area and length features; the shape definitions were obtained using the aspect ratio, compactness, and circularity; the signal strength was measured with the intensity feature.

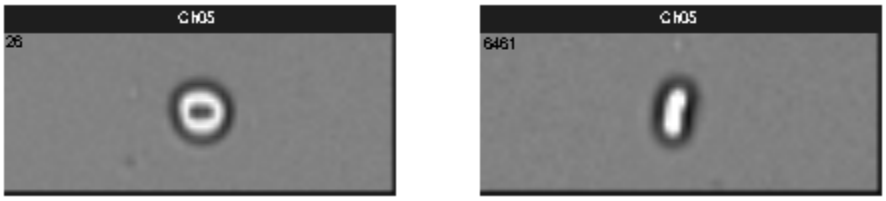

Figure 23. Example of discrimination of erythrocytes based on position captured. Left shows erythrocyte "face on" and right shows erythrocyte "sideways" as detected on control samples.

The area and length of the different samples were evaluated. The area feature on the x-axis is shown in μm and it is calculated by converting the number of pixels of the mask region in the image to area (1 pixel =0.25 μm^2). The length feature was used to

analyze the longest dimension of each cell. This was critical for comparison and to measure the diameter accurately while accounting for erythrocytes biconcave shape and the different cell orientations in the images (Figure 23).

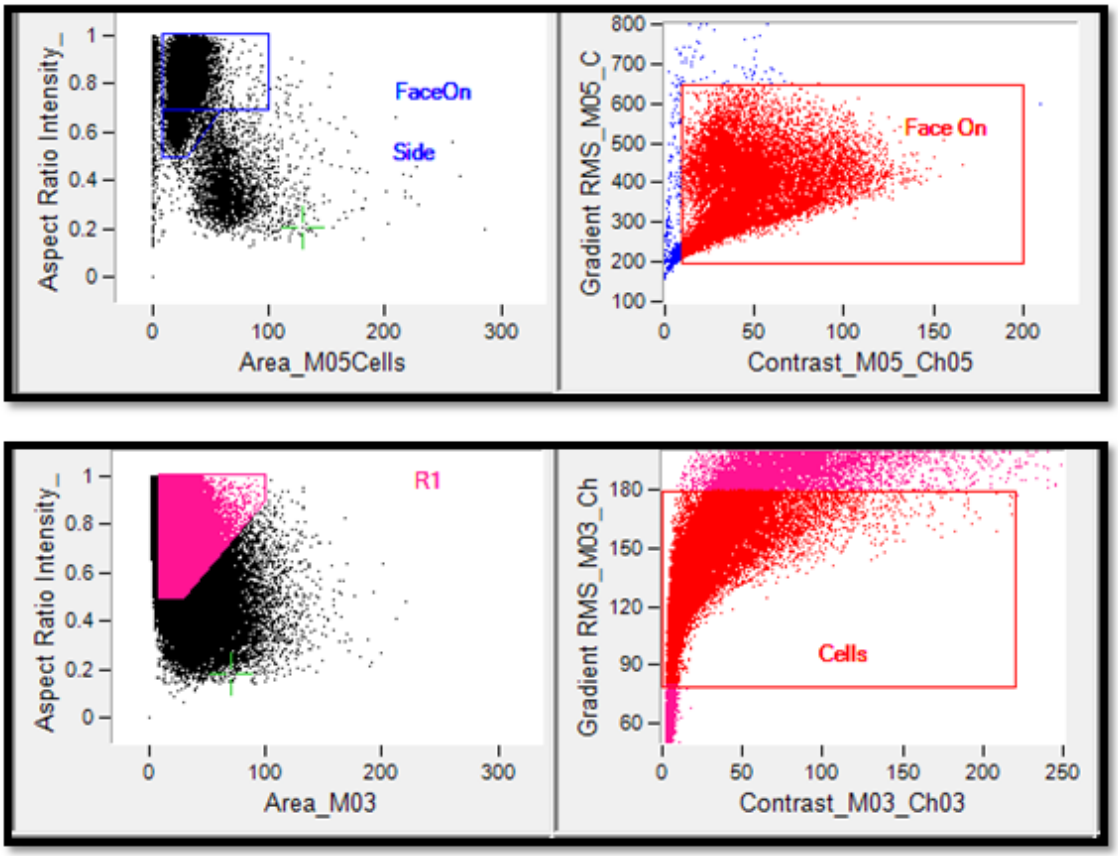

Figure 24. Example of analysis template. Top: Control and preswelling sample of template. Bottom: Sample template for hypotonic dilution population.

First the single cells which fall within the area and aspect ratio intensity parameters used for the control native erythrocytes were defined (Figure 24 top). The approximate

area expected for a "face on" cell with a diameter between 4 and 8 μm was calculated to be between 10 and 51 μm^2. However, to capture erythrocytes and erythrosensor abnormalities, an area region between 10 and 100 μm was used for all the samples. An aspect ratio intensity value between 0.9-1 indicates roundness of the fluorescent image. However, because of the biconcave shape of native erythrocytes the aspect ratio intensity can be lower. For the "face on" a cut out of 0.7 was determined. For the "sideways" samples the limitation for the gate were set between 0.5 and 0.7 was used.

The initial native erythrocytes scatter plot (Figure 24 top) revealed a population of interest concentrated between 10-100 in the area and 0.5-1 in the aspect ratio intensity. The population in the control and preswelling samples showed events facing front labeled "face on" lie between 0.7-1 in the aspect ratio side. While the events facing sideways lie between 0.5-0.7 in the aspect ratio side. The distribution of the population in the hypotonic dilution plot is seen clustered (Figure 24 bottom). Populations are indistinguishable one from another.

In addition, the native erythrocytes, control and the preswelling sample exhibited two populations. Table 2 shows that between 7-10% of events were capture in a "sideways" position and between 71-73% of events were captured in a "facing on" position. Remarkably different to the undetected "sideways" position and 25% "face on" orientation of the hypotonic dilution events.

Table 2. Samples and percentage of cells in face on and sideways positions

Sample	Cargo	Face On	Sideways
Control Naive	No Cargo	72%	8%
Control Preswelling	No Cargo	71%	7%
Control Native + FITC	FITC-glygly	73%	10%
Preswelling	FITC-glygly	76%	9%
Hypotonic Dilution	FITC-glygly	25%	None

Histograms were used to evaluate the population on interest dimensions, morphology and fluorescence signal intensity. The results corroborated the two orientations findings for the erythrocytes with biconcave shape, face on and sideways. Thus, the histogram shows the events orientation as follows: "sideways" orientation in gray while the "face on" orientation are shown in red for the following graphs.

The area and length features were used to evaluate the dimensions of the samples. The population distribution and the average for the area and length features were different between the native erythrocytes, and control samples, and the hypotonic dilution erythrosensors. However, the native erythrocytes, control and preswelling samples exhibited similarities in the two populations distribution found ("sideways" and "face on") and in area and length of the events. The native erythrocytes face on sample had an area of 28.21 μm^2 +/-7.96. The hypotonic dilution erythrosensors exhibited an area average of 9.55 μm^2 +/-13.95, while the average area for preswelling erythrosensors facing on was 28.35 μm^2 +/- 7.78. The hypotonic dilution shows greater variability and a bimodal population distributed up to 100 μm^2 in terms of the area (Figure 24). With respect to the

length the events in the hypotonic dilution correlates with normal bovine diameter (approx. 5.8 μm) and the previous work that showed a normal diameter in hypotonic dilution erythrosensors. For the control, native erythrocytes face on and sideways the average length was 5.98 μm +/- 0.9185 and 5.470 μm +/- 0.6189 respectively. The hypotonic dilution erythrosensors exhibited a length averaging of 5.764 μm +/-1.479 while the preswelling erythrosensors show an average length for face on and sideways of 5.98 μm +/- 0.8959 and 5.425 μm +/- 0.6103. Throughout the flow cytometry work the sideways population present in control native erythrocytes and preswelling is absent in the hypotonic dilution analysis. Since the hypotonic dilution erythrosensors acquire a spherical shape (chapter III), this morphological change could explain why a sideways population is not recognizable.

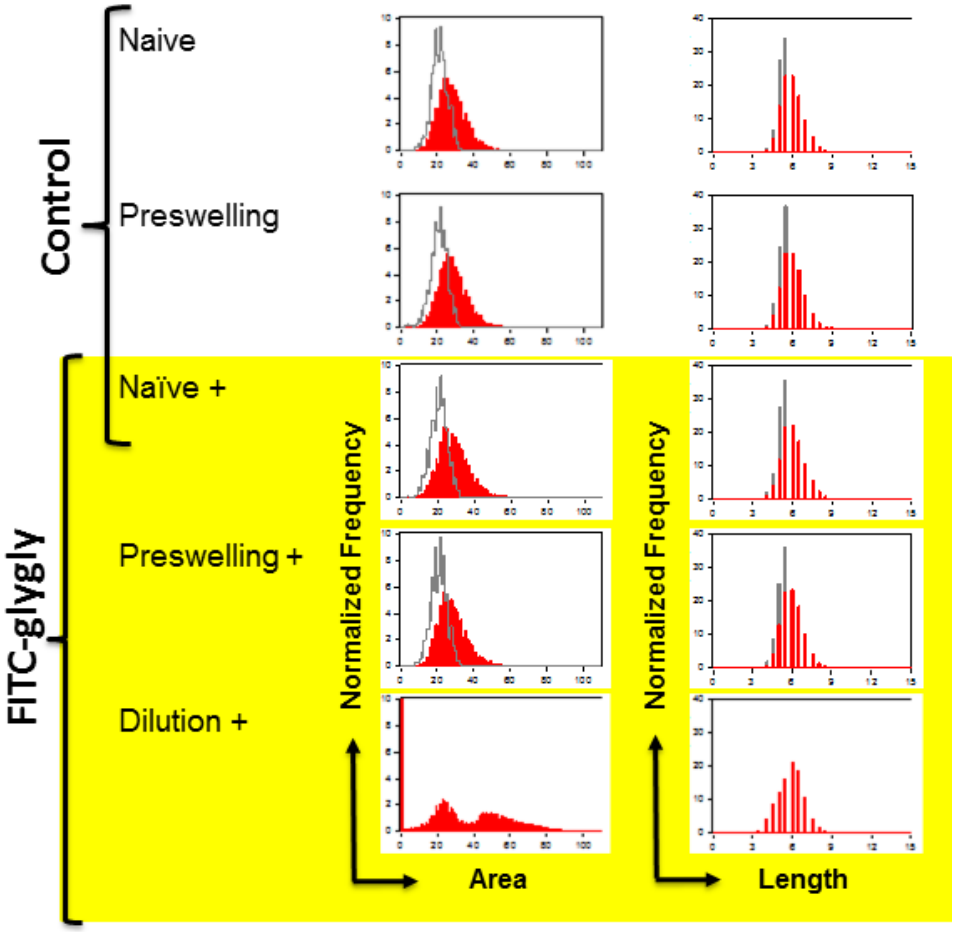

Figure 25. Dimensions of native erythrocytes, controls and erythrosensors. Control samples include native erythrocytes, preswelling erythrosensors without any FICT-glygly and native erythrocytes mixed with FITC-glygly having undergone a loading procedure. Preswelling and hypotonic dilution erythrosensors with FITC-glygly as cargo were also analyzed.

Erythrocyte distinguished from other cells by their enucleation and biconcave morphology. These unique features contribute significantly to their mobility and function. The aspect ratio, compactness and circularity features were used to identify potential changes in these characteristics.

The aspect ratio (length to width ratio) is a feature use to detect elongation or roundness of the event by dividing the minor axis and the major axis. Thus, it was used to discriminate between single (equal width and height) and double events in an image and to determine the shape of the samples. The controls show 65% of events have an aspect ratio close to 1.0, indicating mainly rounded events in the cells "face on". Native erythrocytes mixed with FITC-glygly and the preswelling erythrosensors with cargo FITC-glygly presented a left shift towards 0.8. The histogram for "sideways" events in the control and preswelling, the histogram shows a left shift towards 0.7 that correlates with the elongated shape of the erythrocyte shape when oriented sideways. The preswelling loaded with FITC-glygly had increased frequency of events between 0.8-1.0, indicating more events with a rounded shape. However, there is a tail in the "facing on" cells below 0.8. The hypotonic dilution exhibits a tail in the graph that extends even more than the tail on the preswelling samples reaching up to 0.6 in the aspect ratio histogram.

To evaluate and compare the morphology of the samples, the compactness and circularity features were used. These features were used to identify non-circular events in the dot plot. The circularity feature measures the deviation from the image and the mask of a circle (how much the radius varies). Rounder events have low radial variance and a high circular score. The feature scores the events between 0 and 30, the higher the value, the closer the shape is to a circle. If the shape deviates from a circle, is found to be ruffled or elongated, the circularity score will be low (high radial variance). The compactness, measuring the compression, the higher the value the more condensed is the event. In terms

of circularity, the control samples and the preswelling had an average 10.85 +/- 2.67 and 10.98 +/- 2.64 score, respectively. The hypotonic dilution shows drastic differences with a 6.94 +/- 4.81 score. The hypotonic dilution samples exhibited a lower circularity value and more variation, which indicates irregularities in the shape.

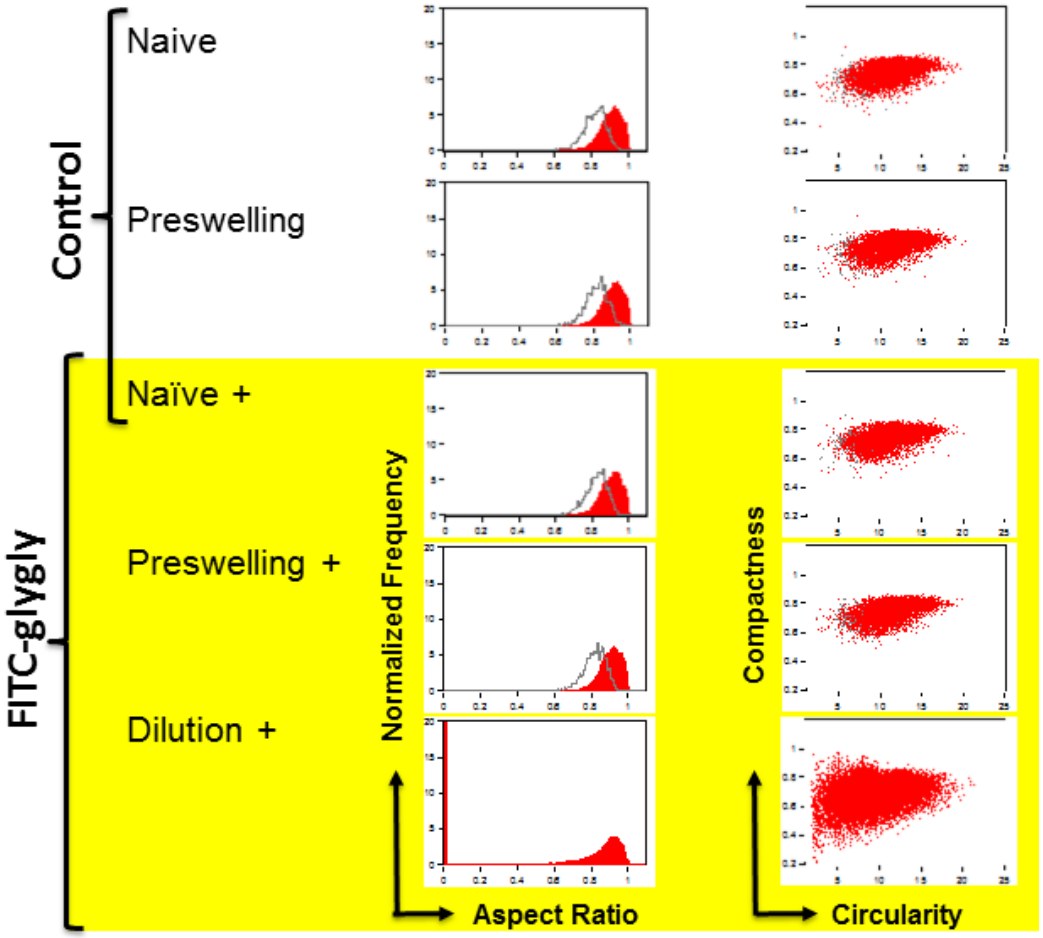

Figure 26. Morphology of native erythrocytes, controls and erythrosensors. Samples was determined by the aspect ratio and circularity.

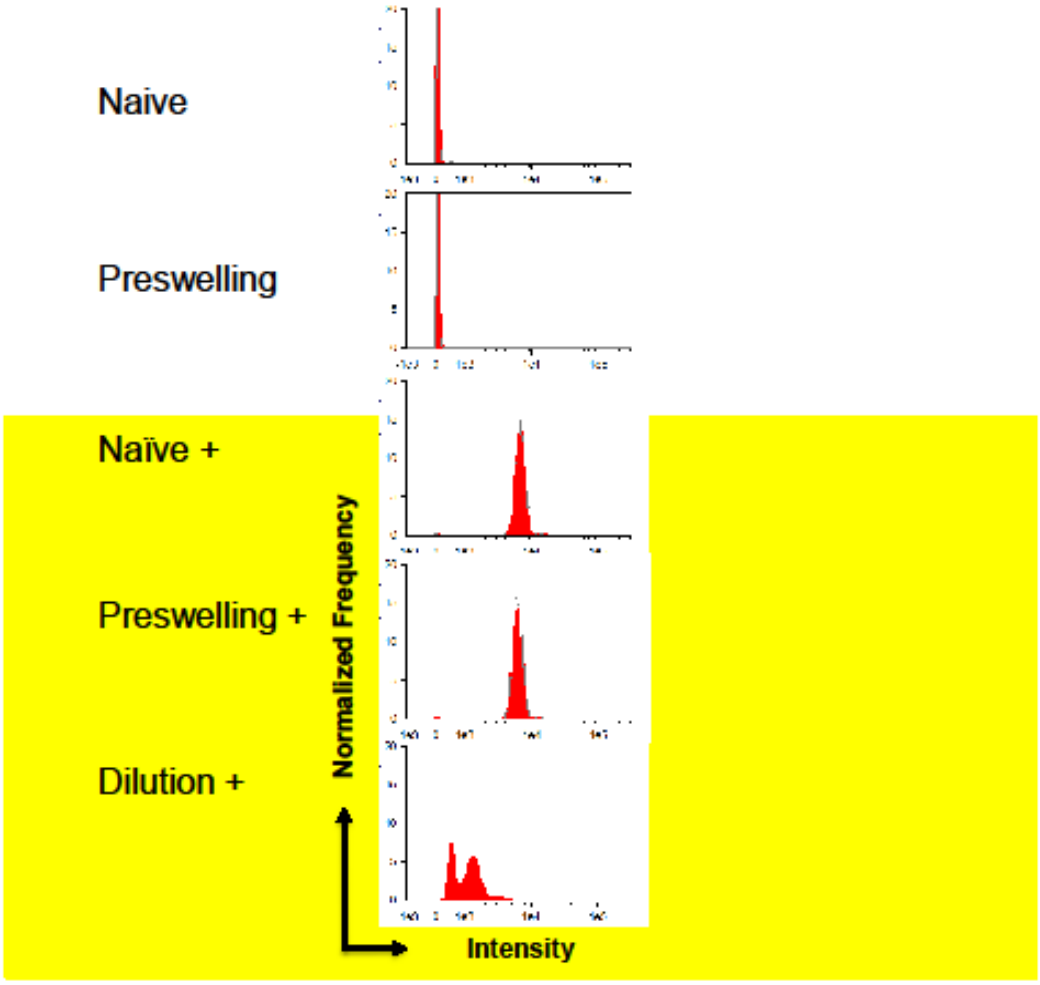

Figure 27. Fluorescence signal strength in erythrosensors. Erythrocytes were loaded via preswelling and hypotonic dilution.

The intensity feature use to evaluate the fluorescence signal strength for the samples subtracts the average background pixel value from the area of interest (Figure 27 and Figure 28). As expected the controls without FITC-glygly the sample had no fluorescence signal. Confirming that the fluorescence signal is not product of auto-fluorescence or other non-specific reactions. On one hand, the hypotonic dilution, just as

seen before, exhibits variability in the fluorescent signal with an average intensity of 1386 +/- 2200.46. In fact, three peak are evident in the histogram. On the other hand, the preswelling with FITC-glygly technique shows a single peak with a 4-fold increase in the signal with an average intensity of 6577.68 +/-2034.78. One-way ANOVA revealed significant difference among all the samples except the control naïve and the preswelling without FITC which had no significant difference. The error bar represents the standard deviation $P<0.0001$. A striking finding was the control naïve erythrocytes mixed with FITC-glygly procedure showed fluorescent signal in the events and even a shift towards a stronger fluorescent signal with an average intensity of 6704.94 +/-1114.11.

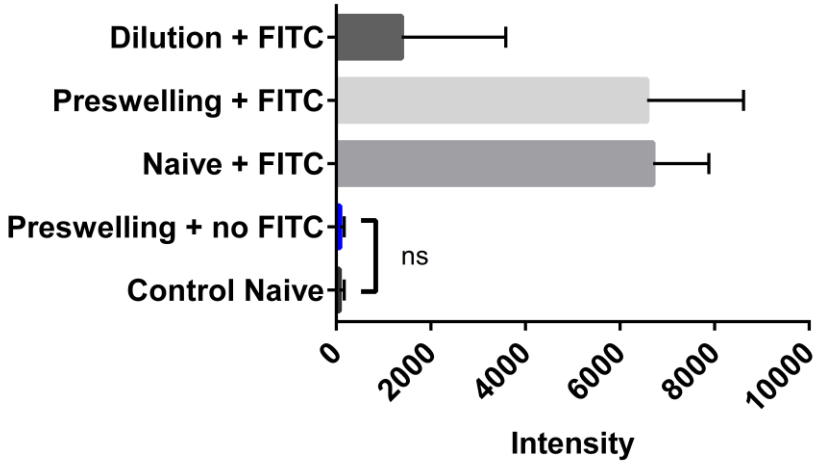

Figure 28. Summary of average intensities in samples. The populations face on and sideways were used for the overall average.

Subsequently, the bright field and fluorescent images of the samples were examined to understand the evidence of the florescence signal detected in the native erythrocytes mixed with FITC-glygly without having undergone a loading procedure (Figure 29). The naive erythrocytes mixed with FITC-glygly exhibit similar morphology to the native erythrocytes. However, the fluorescence signal seems irregular and superficial when compared to the preswelling loaded with FITC-glygly. If we now turn to the hypotonic dilution sample, the three differing populations in the sample can be identified in the images. Furthermore, the misshapen and low contrast events in the bright field and the fluorescence values variability in the intensity were upheld. The preswelling with and without FITC-glygly exhibit similar morphology and size. In fact, the fluorescence in channel 3 appears to be the only difference. The preswelling sample loaded with FITC-glygly also shows a uniform loading. To further characterize the results from the naïve erythrocytes mixed with FITC-glygly without having undergone a loading procedure, the reactivity of FITC and FITC-glygly with naïve erythrocytes was investigated.

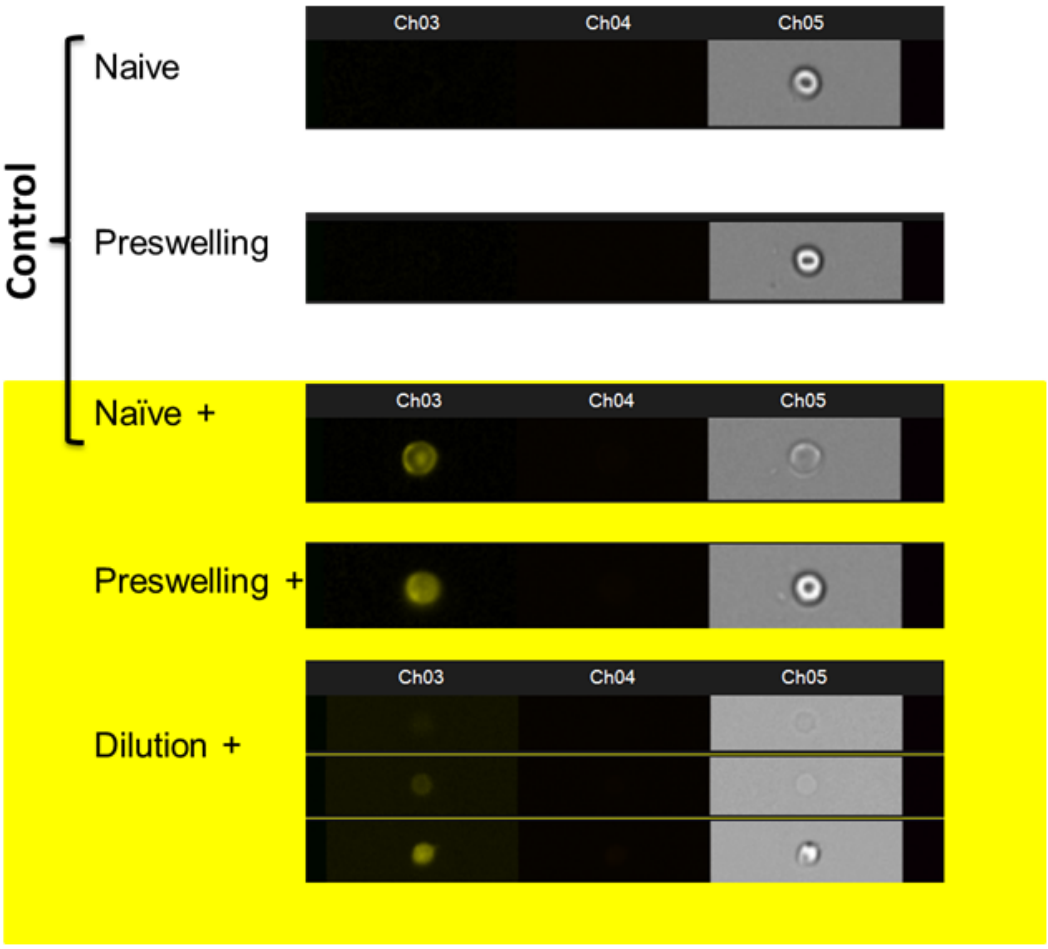

Figure 29. Examples of image file data for each sample condition. Channel 3 show the fluorescence image and channel 5 shows the corresponding bright field image.

Naïve erythrocytes mixed with FITC-glygly exhibited a shift towards greater signal strength. This raised the question as to whether this is due to spontaneous loading (endocytosis), or non-specific interactions with the membrane. To answer this question, naïve erythrocytes were mixed with different FITC-glygly and FITC only formulations.

FITC can react with amine groups on proteins. Results from control naïve erythrocytes mixed with FITC and FITC-glygly show that when FITC is mixed with erythrocytes it can lead to reactivity with the cells which exhibit a strong fluorescent signal. We investigated at FITC-glygly diluted in dH2O or PBS mixed with naïve erythrocytes and found there was no increase in the fluorescence signal (
Figure 30). Indicating the possibility that the control with FITC-glygly must have unreacted FITC, leading to non-specific association with membrane proteins and, thus, a strong signal in the naïve erythrocytes mixed with FITC-glygly. A representative maximum intensity projection and Z-Stack of naïve erythrocytes mixed with FITC is shown in figure (Figure 30). Bovine erythrocytes were used to create a z-stack with step size between images shown of 1 microns.

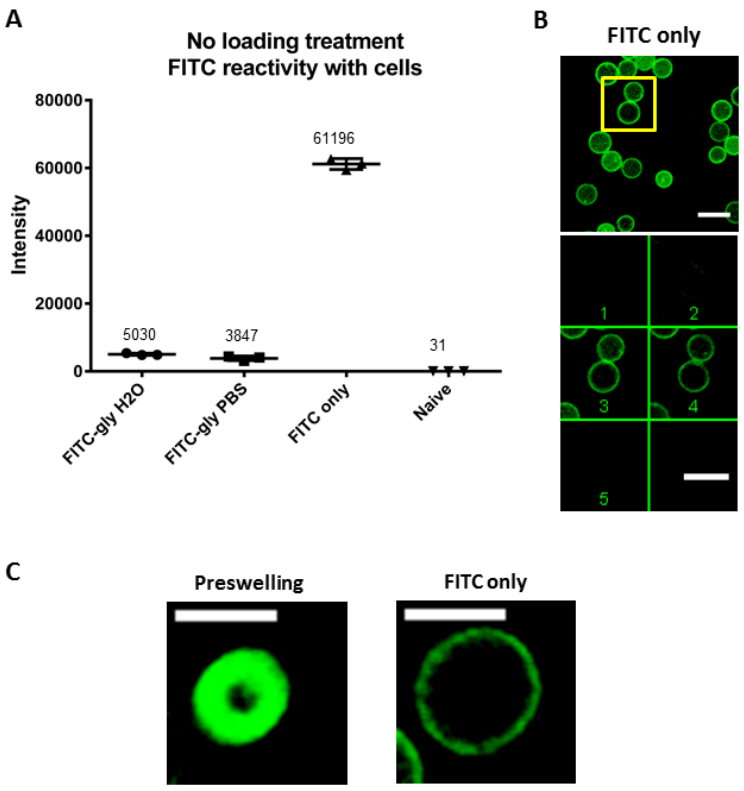

Figure 30. FITC reactivity with erythrocytes. A. naive erythrocytes mixed with FITC-glygly diluted in PBS or dH2O, and FITC only were mixed with native erythrocytes. FITC-glygly reaction was incubated for 2 hours instead of 30 minutes. B. Unconjugated FITC interaction with erythrocytes shown in z-stack with 1 μm step. C. Confocal images showing erythrosensor loaded with FITC-glygly produced via the preswelling technique on the left and the native erythrocytes mixed with just FITC.

The initial investigation aimed to determine if this newly developed method could, in fact, load erythrocytes with fluorescent dye while maintaining innate morphology. The features derived from the individual Image stream data for each condition: controls: naïve, naïve with FITC-glygly and preswelling without FITC-glygly, and the preswelling with

FITC-glygly, were used to construct the principal component analysis (PCA) to achieve an objective statistical method to differentiate between the groups. The parameters analyzed were the area, aspect ratio, circularity, compactness and intensity. The four conditions were plotted, defined by the 1st and 2nd principal component functions. PCA reduces the data dimensions for visualization in a two-dimensional plot (Figure 31). In the figure, blue represents the naïve erythrocytes (Naïve), red shows the preswelling loading using with FITC (Preswelling), green shows the preswelling without FITC (PreNoFITC) and maroon represents the naïve erythrocytes mixed with FITC-glygly (NF).The results show the samples without FITC-glygly locate in the same region in the plot, indicating that the preswelling without FITC-glygly and the naïve erythrocytes compare and the loading procedure does not alter the parameters analyzed. Preswelling without FITC-glygly and naïve erythrocytes with FITC-glygly exhibit the same characteristics in terms of the variables evaluated (dimension, morphology). The preswelling loading using FITC-glygly groups in a specific form indicating that the fluorescence is a factor that can be utilized to differentiate the samples. Once the fluorescence in analyzed the population shifts to the right and aligning the fluorescent samples in the same region. The aggrupation of the samples with and without FITC-glygly is seen.

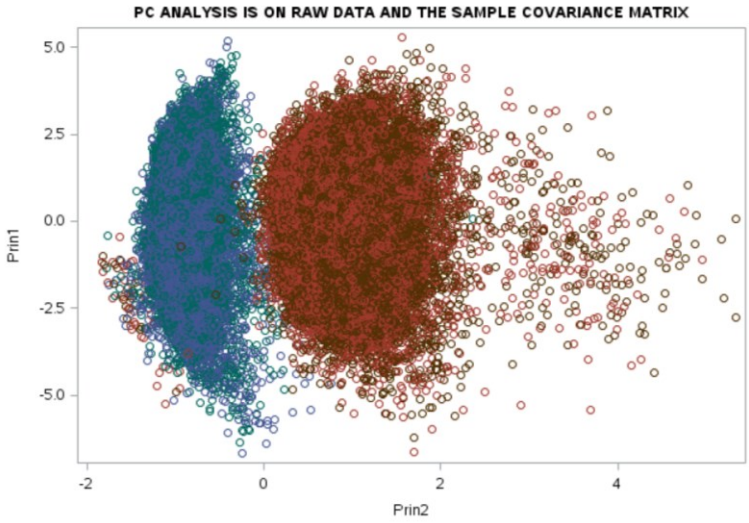

Figure 31. Principal component analysis (PCA). The multiparameters analysis was used on naïve/without FITC, and preswelling with/without FITC samples. The color of the symbols represent: ○ naïve erythrocytes, ○ preswelling treatment no FITC, ○ naïve erythrocytes mixed with FITC-glygly, ○ Preswelling treatment loaded with FITC.

To visualize preswelling erythrosensors confocal imaging was used to confirm morphology and fluorescent signal. A representative image of erythrosensors is shown in Figure 32. The confocal imaging was collected immediately after loading procedure. The erythrosensors seems to mimic the control erythrocytes size. FITC-glygly loading is shown in green color. Overlays of the transmission and fluorescence channels are shown in the right.

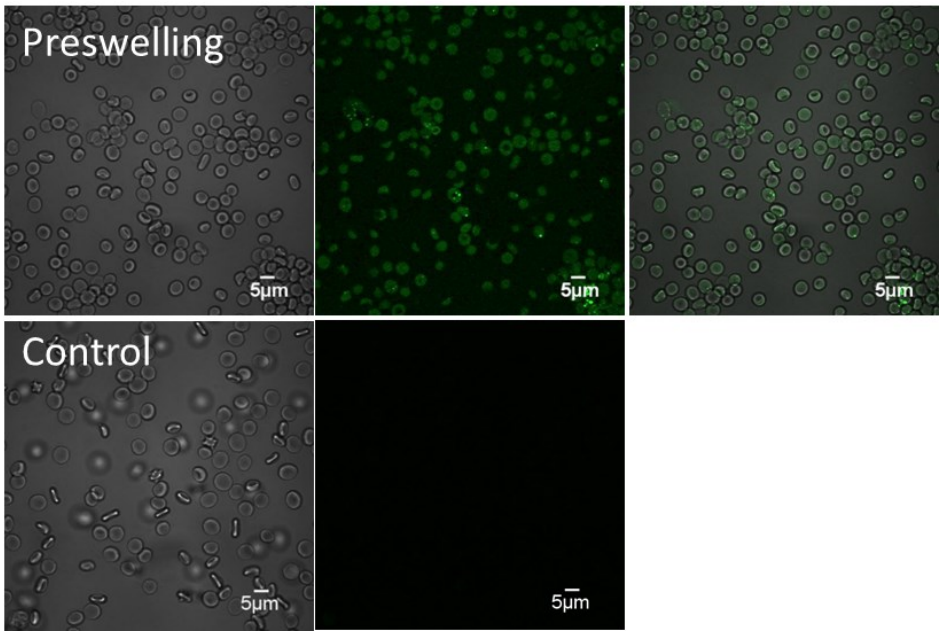

Figure 32. Confocal imaging reveals uniform loading and shape of erythrosensors.

Volumetric analysis of bovine erythrocytes loaded via preswelling revealed volume-loading through the erythrosensors (Figure 33). An example of a maximum intensity projection and the region selected for further analysis is shown in the yellow square in the top image. The Z-stack is shown with a size of 1 micron. The fluorescence image shows the cells were loaded with FITC-glygly.

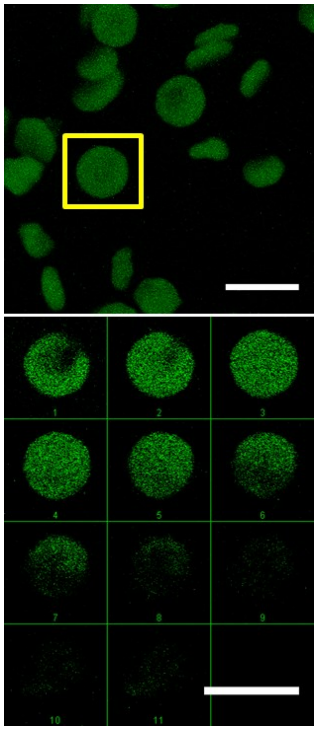

Figure 33. Maximum intensity projection and z-stack of bovine erythrosensor.

Looking at the hemoglobin retained and comparing with the hemoglobin levels achieved with other loading procedures, the mean concentration between erythrosensors loaded via preswelling and the control erythrocytes is comparable (Figure 34). As seen in Chapter III, hypotonic dilution erythrocytes retained only 11% of hemoglobin concentration, while electroporation retained 60% of hemoglobin. In addition, the measured hemoglobin concentration of 8.99 g/dL +/- 0.655 matches the concentration of normal bovine erythrocytes. This will help the erythrosensors mimic erythrocyte characteristics and functions while functionalized as a sensor carrier.

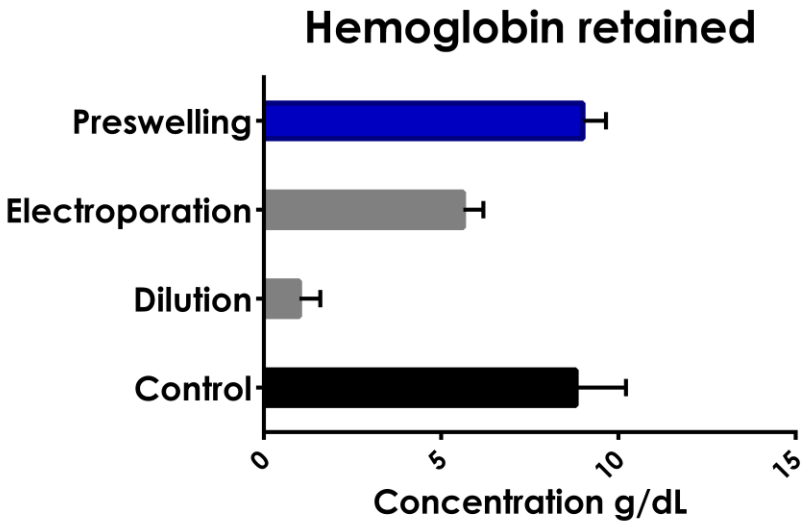

Figure 34. Hemoglobin retained in erythrosensors loaded via preswelling.

Strong evidence of successful loading via the preswelling technique led us to attempt loading human erythrocytes. The yellow box in the maximum intensity projection shows the erythrosensors studied (Figure 35). The procedure was tailored to human erythrocytes for loading FITC-glygly cargo. The resulting data shows volume loaded erythrosensors with an average area of 55.26 +/- 14.06 and an average diameter of 8.906 +/- 1.063. Normal human erythrocytes are reported to have a diameter between 6-8 microns. These results give the first glimpse of how the developed technique can be tailored to load erythrocytes from different species, while maintaining the characteristics critical for prolonged *in-vivo* survival.

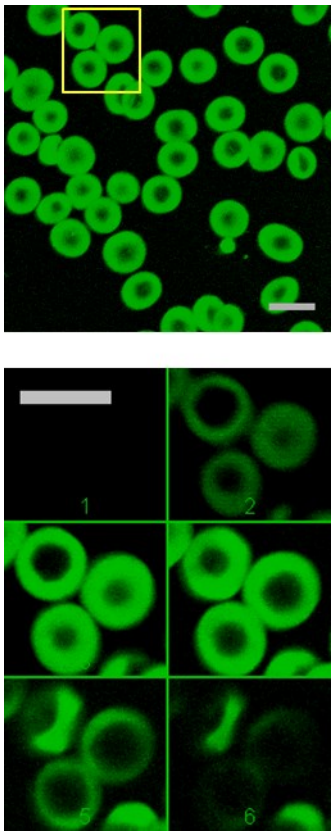

Figure 35. Preswelling procedure on human erythrocytes. Top image shows the maximum intensity projection and the yellow box indicates z-stack pictured in the bottom with a step size of 1 µm.

Loading of an NIR dye using the preswelling technique was evaluated. Indocyanine green (ICG) is an FDA approved dye commonly used in diagnostic applications. Structurally ICG is a larger molecule than FITC, with infrared absorbing properties (800 nm) and little absorption in the visible range. It is an NIR dye with applications ranging from imaging-guided photo thermal therapy, contrasting agent for angiography [109-1110].

To tailor the preswelling procedure to load a molecule larger than the model cargo FITC-glygly into human erythrocytes, different osmolarity conditions were evaluated, and a standard curve was constructed. The implementation of ICG as a model cargo was limited by the lack of an infra-red detection system on the microscope. Naive erythrocytes, erythrosensors created via preswelling loaded with ICG and a control sample which underwent preswelling procedure without ICG were evaluated using spectrophotometric analysis. At the end of the procedure the supernatant was also saved. After several sample washes, erythrosensor entrapment of ICG was evaluated by cellular rupture in deionized water. The supernatant for each experimental sample after the procedure was also analyzed to validate with results for cargo entrapment. For an initial concentration of 20 µg ICG per 1 ml of human erythrocytes, an entrapment efficiency (the percent of cargo entrapped into erythrosensors) of 48.5% was found.

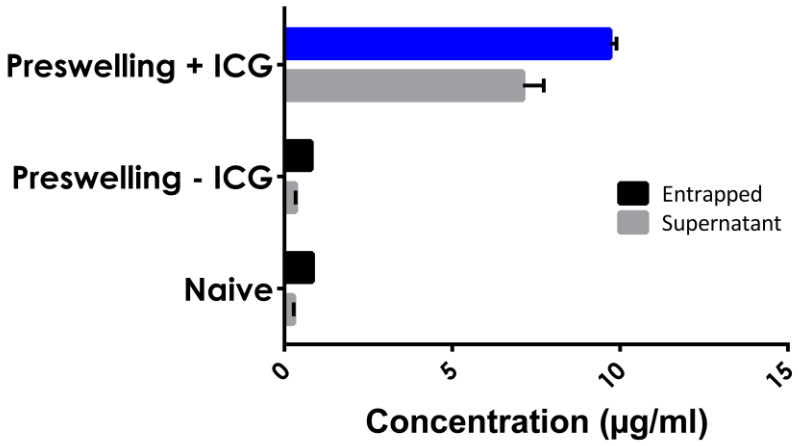

Figure 36. Adapting preswelling procedure to NIR dye ICG.

Discussion

Erythrocyte pathological abnormalities (dimensional and morphological) have been extensively investigated. Safeuki et al. (2012) use image flow cytometry to show splenic entrapment of erythrocytes with changes in these features [91,112]. Motivated by these findings, the size, morphology and fluorescence signal of erythrosensors were evaluated. Prior studies noted the importance of maintaining hemoglobin levels, to conserve the characteristics that make erythrocytes attractive sensor carriers [13,14].

A strong relationship between size/morphology and the survival of erythrocytes has been reported in literature [112]. The current study's findings correlate with our previous results showing the abnormal morphology that the hypotonic dilution procedure causes to the erythrocytes. While the erythrosensors maintain a size in the region of normal erythrocytes, the biconcave shape alters to a spherical form. Thus, we aim to develop a procedure that maintains the size and shape of normal erythrocytes.

Based on previous work where reverse osmosis is used to load erythrocytes, we developed a rapid technique to gently load fluorescent dye. Using the preswelling loading procedure we improve hemoglobin retention and homogeneity of loading of FITC-glygly. The size and shape of erythrosensors matched well with the measurements of normal erythrocytes. In addition, the narrow fluorescent signal exhibited a 3-fold increase over the hypotonic dilution.

Surface coating of erythrocytes with fluorescent molecules have been well studied to answer biological questions, and understand erythrocytes' properties. Although the erythrocyte membrane is considered a semipermeable membrane, it is highly selective. Through osmosis, a solvent such as dH2O diffuses into a more concentrated solution to reach equilibrium in the concentration of solutes. In erythrocytes subjected to a hypotonic solution, water diffusing out may account for the preswelling procedure functioning to load erythrocytes with cargo while causing minimal changes.

The high affinity for proteins and pH response makes FITC an ideal compound to investigate the extracellular pH tracking. However, these characteristics also present issues of non-specificity association of reactant FITC with membrane proteins. These properties may explain the control naïve exhibiting a strong fluorescent signal when mixed with FITC-glygly –and potentially unreacted FITC. In the past, FITC has routinely been conjugated with glycylglycine, however, the FITC-glygly conjugation process was not followed by further purification for removal of unreacted FITC. FITC is a charged molecule. FITC-glygly conjugation leads to net negative charges resulting in background and non-specific binding to positive surfaces. Unbound FITC should be removed by a suitable purification method such as gel filtration. Also, blocking with 1% BSA PBS (1% bovine serum albumin diluted in 1X PBS) the membrane protein could prevent non-specific interactions. Other FITC characteristics that may hinder the analysis include: collisional quenching of fluorescence, photo bleaching, and quenching in acidic conditions and instability in water (subsequently aqueous media).

The most interesting finding was the highly controllable, adaptable and scalable procedure to load erythrosensors with fluorescent cargo. We successfully loaded FITC-glygly into human erythrocytes. These loaded erythrocytes exhibited similar characteristics to normal erythrocytes and bovine erythrocytes loaded with FITC-glygly using the preswelling technique.

CHAPTER V

SUMMARY, LIMITATIONS AND OUTLOOK

Using erythrocytes as sensor carriers, we explored their dimensions and morphology as well as the biological features required for long term monitoring. In chapter II, loading procedures were optimized around encapsulation of FITC-glygly in erythrocytes. Erythrosensors loaded via hypotonic dilution and electroporation lost 89% and 46% of the total hemoglobin, respectively. In terms of fluorescence, erythrosensors loaded via hypotonic dilution had 4X more fluorescence intensity than cells loaded using electroporation. The results of these studies suggest that hemoglobin levels and cargo loading concentrations are inversely related using these techniques. These findings are particularly useful as the basis to standardize the characterization erythrosensors used in an erythrocyte-based sensing system.

Since the overall goal of this work was to study FITC-glygly loaded erythrocytes and hypotonic dilution was shown to have the most fluorescence per cell, the work in chapter III focused on providing deeper insight into cellular changes in erythrosensors loaded via hypotonic dilution. Initially, the capacity of erythrosensors to entrap the optical sensor dye was demonstrated in both rat and bovine erythrocytes. Micrographs of the resulting population showed erythrosensors with varying levels of FITC-glygly encapsulated and 3D images render insight into erythrosensor shape.

From the fluorescent images, it was apparent that the cell underwent both, morphological and topological changes. The use of AFM to characterize erythrosensors provided a route to explore these changes. Erythrosensors loaded via hypotonic dilution shrink, and their surface topography became rugged. Until now, the morphological changes erythrosensors underwent when subjected to the hypotonic loading procedures were unknown. The results showed that the height, and diameter size of the cell decreased. Native erythrocytes were found to have a 5-6 μm diameter range and 1-2 μm height range. FITC-glygly loaded erythrosensor height and diameter size were found to have decreased by an average of 1 μm in both diameter and height. Furthermore, the surface of erythrosensors was found to be up to twice as rough as the surface of native erythrocytes. After verifying erythrosensors integrity via AFM, it was confirmed that erythrosensors loaded via hypotonic dilution lost standard erythrocyte architecture. The erythrosensor cellular characteristics found in this study, could limit their ability to circulate through small capillaries, obstruct oxygen transportation and lead to rapid clearance.

Reschsteiner and Tsang et al. first showed erythrocyte preswelling procedures loading Calcein or FITC-BSA as cargo and exploring successive swelling with equilibration periods (2-5 min) followed by restoration of its tonicity with a NaCl solution for 60 min at 40˚ C [99,102]. Inspired by the simplicity of the preswelling procedure, a rapid procedure was developed, considering recent clinical finding to conserve the characteristics of the erythrocyte. In addition, loading of FITC-glygly and NIR dye, such as ICG in human erythrocytes was demonstrated. The results showed that the method

chosen for erythrosensor production will have a critical impact on the sensor carrier ability to mimic normal erythrocytes.

Limitations

There are a number of questions unanswered. For example, how does FITC concentration loading affect hemoglobin concentration and loading efficiency using the preswelling technique? Another question is how the oxygen transportation function is affected by the procedure? The location (external, internal, or transmembrane association) of the sensing probes could also affect the overall functionality.

Other erythrocytes biological characterization should also be considered to improve the effectiveness of erythrocytes as erythrosensors. Well-studied erythrocyte features such as the membrane composition and the integrity should be analyzed. In addition, new strategies to load erythrocytes and verify the integrity of the resulting erythrosensors in physiological conditions should be explored and evaluated using the methods developed here.

Outlook

A blood sample could provide the autologous erythrocytes essential to the long term blood analyte monitoring system erythrosensors. Although blood samples are easy to collect, there are drawbacks for patients such as, diabetics: pain, and scarring tissue could lead to inflammation and other complications. This study of a minimally invasive

platform for measurements of blood molecules such as glucose was advanced. Common erythrocytes loading procedures were evaluated and an alternative loading procedure were advanced. However, there is also an opportunity to investigate loading of circulating erythrocytes *in-vivo*, without having to take the invasive blood sampling.

Every second erythrocytes are destroyed in the RES. Although erythrocytes are abundant, it is worthwhile to investigate loading of other populations of cells such a lymphocyte to detect, not only analytes of interest but maladies biomarkers. This approach can be used for monitoring of progression, and or management of diseases that are currently managed via blood sampling.

The cell morphology of erythrocytes has been attributed to the need to transport oxygen, giving erythrocytes more area while being able to squeeze through capillaries. Thus, maintaining the morphology is not only critical to guaranteeing prolonged survival, but it could also be potentially beneficial to maximize the area and the transportation of the cargo, in this case FITC-glygly. In addition, it is essential to achieve the maximum concentration per cell to translate it into circulatory signal emission.

Erythrocytes respond to osmolarity changes and a number of probes for sensors can be entrapped during the intracellular equilibration period. Carrier erythrocytes have been used for the treatment of adenosine deaminases (ADA) deficiency, which causes immunodeficiency. Potential toxicity and immune response is reduced when using carrier

erythrocytes encapsulating ADA therapy compared to the bolus dye systemic administration in the blood stream. Biocompatibility, biodegradability, and low toxicity makes erythrocytes attractive for use as a drug transportation system. Thus, these protective features are also sought after in the implementation of carrier erythrocytes for biosensing applications. Erythrocytes carriers and erythrosensors can encapsulate different molecules, and they offer cargo protection.

In the future, preswelling erythrosensors' ability to sense glucose while maintaining native cellular and mechanical properties, should be evaluated. Confocal microscopy and AFM have been used to study erythrocytes extensively. In this thesis, I developed protocols to characterize erythrosensors. Despite its exploratory nature, this study offers insight into standardizing methodologies to assess carrier erythrocytes and erythrosensors cellular features.

A limiting factor with fragile biological samples, such as erythrocytes, is the storage limitations which also impacts the ability to implement in clinical practice. Maintaining the physiological characteristics, as well as the fluorescence signal is critical for the study and clinical application of erythrosensors.

REFERENCES

[1] Gregg EW, Boyle JP, Thompson TJ, Barker LE, Albright AL, Williamson DF. Modeling the impact of prevention policies on future diabetes prevalence in the United States: 2010–2030. Popul Health Metr 2013;11:18.

[2] Pettitt DJ, Talton J, Dabelea D, Divers J, Imperatore G, Lawrence JM, et al. Prevalence of diabetes in U.S. youth in 2009: the SEARCH for diabetes in youth study. Diabetes Care 2014;37:402-408.

[3] Shin J, Park H, Cho S, Nam H, Lee K. A correction method using a support vector machine to minimize hematocrit interference in blood glucose measurements. Comput Biol Med 2014;52:111-118.

[4] Cheng W, Lin C, Wu T, Su C, Hsieh M. Calibration of glucose oxidase-based test strips for capillary blood measurement with oxygen saturated venous blood samples. Clinica Chimica Acta 2013;415:152-157.

[5] Freckmann G, Freckmann A, Baumstark N, Jendrike E, Zschornack S, Kocher J, et al. System Accuracy Evaluation of 27 Blood Glucose Monitoring Systems According to DIN EN ISO 15197. Diabetes technology & therapeutics 2010;12:221-231.

[6] Casas Oñate ML, Montoya Martínez D. ¿Son fiables los medidores de glucemia capilar?. Avances en Diabetología 2012;28:110-113.

[7] Moser EG, Morris AA, Garg SK. Emerging diabetes therapies and technologies. Diabetes Res Clin Pract 2012;97:16-26.

[8] Vashist SK. Non-invasive glucose monitoring technology in diabetes management: A review. Anal Chim Acta 2012;750:16-27.

[9] Wang J. In vivo glucose monitoring: Towards 'Sense and Act' feedback-loop individualized medical systems. Talanta 2008;75:636-641.

[10] Sanz V, de Marcos S, Galbán J. A blood-assisted optical biosensor for automatic glucose determination. Talanta 2009;78:846-851.

[11] Marrero D, Pan Q, Barrett-Connor E, de Groot M, Zhang P, Percy C, et al. Impact of diagnosis of diabetes on health-related quality of life among high risk individuals: the Diabetes Prevention Program outcomes study. Quality of Life Research 2014;23:75-88.

[12] Wittenborn JS, Zhang X, Feagan CW, Crouse WL, Shrestha S, Kemper AR, et al. The Economic Burden of Vision Loss and Eye Disorders among the United States Population Younger than 40 Years. Ophthalmology 2013;120:1728-1735.

[13] Ritter SC, Milanick MA, Meissner KE. Encapsulation of FITC to monitor extracellular pH: a step towards the development of red blood cells as circulating blood analyte biosensors. Biomedical optics express 2011;2:2012-2021.

[14] Milanick MA, Ritter S, Meissner K. Engineering erythrocytes to be erythrosensors: First steps. Blood Cells, Molecules, and Diseases 2011;47:100-106.

[15] McNichols RJ, Cote GL. Optical glucose sensing in biological fluids: an overview. J Biomed Opt 2000;5:5-16.

[16] Dodge JT, Mitchell C, Hanahan DJ. The preparation and chemical characteristics of hemoglobin-free ghosts of human erythrocytes. Arch Biochem Biophys 1963;100:119-130.

[17] Schwoch G, Passow H. Preparation and properties of human erythrocyte ghosts. Mol Cell Biochem 1973;2:197-218.

[18] Clark LC, Lyons C. Electrode systems for continuous monitoring in cardiovascular surgery. Ann N Y Acad Sci 1962;102:29-45.

[19] Turner AP, Pickup JC. Diabetes mellitus: biosensors for research and management. Biosensors 1985;1:85-115.

[20] Clarke S, Foster J. A history of blood glucose meters and their role in self-monitoring of diabetes mellitus. Br J Biomed Sci 2012;69:83-93.

[21] Clarke WL, Cox D, Gonder-Frederick LA, Carter W, Pohl SL. Evaluating clinical accuracy of systems for self-monitoring of blood glucose. Diabetes Care 1987;10:622-628.

[22] Cote GL. Noninvasive and minimally-invasive optical monitoring technologies. J Nutr 2001;131:1596S-604S.

[23] American Diabetes Association. Standards of medical care in diabetes--2013. Diabetes Care 2013;36 Suppl 1:S11-66.

[24] Aye T, Block J, Buckingham B. Toward closing the loop: an update on insulin pumps and continuous glucose monitoring systems. Endocrinol Metab Clin North Am 2010;39:609-624.

[25] Wisniewski N, Moussy F, Reichert W. Characterization of implantable biosensor membrane biofouling. Fresenius J Anal Chem 2000;366:611-621.

[26] Nichols SP, Koh A, Storm WL, Shin JH, Schoenfisch MH. Biocompatible materials for continuous glucose monitoring devices. Chem Rev 2013;113:2528-2549.

[27] Keenan DB, Mastrototaro JJ, Zisser H, Cooper KA, Raghavendhar G, Lee SW, et al. Accuracy of the Enlite 6-day glucose sensor with guardian and Veo calibration algorithms. Diabetes technology & therapeutics 2012;14:225-231.

[28] Christiansen M, Bailey T, Watkins E, Liljenquist D, Price D, Nakamura K, et al. A new-generation continuous glucose monitoring system: improved accuracy and reliability compared with a previous-generation system. Diabetes technology & therapeutics 2013;15:881-888.

[29] Grainger DW. All charged up about implanted biomaterials. Nat Biotechnol 2013;31:507-509.

[30] Li CM, Dong H, Cao X, Luong JHT, Zhang X. Implantable electrochemical sensors for biomedical and clinical applications: progress, problems, and future possibilities. Curr Med Chem 2007;14:937-951.

[31] Torres I, Baena MG, Cayon M, Ortego-Rojo J, Aguilar-Diosdado M. Use of sensors in the treatment and follow-up of patients with diabetes mellitus. Sensors 2010;10:7404-7420.

[32] Hanaire H. Continuous glucose monitoring and external insulin pump: towards a subcutaneous closed loop. Diabetes Metab 2006;32:534-538.

[33] Wei C, Lunn D, Acerini C, Allen J, Larsen A, Wilinska M, et al. Measurement delay associated with the Guardian® RT continuous glucose monitoring system. Diabetic Med 2010;27:117-122.

[34] Hochmuth RM, Marple RN, Sutera SP. Capillary blood flow: I. Erythrocyte deformation in glass capillaries. Microvasc Res 1970;2:409-419.

[35] O-Neill JS, Reddy AB. Circadian clocks in human red blood cells. Nature 2011;469:498-504.

[36] Svetina S, Kuzman D, Waugh RE, Ziherl P, Žekš B. The cooperative role of membrane skeleton and bilayer in the mechanical behaviour of red blood cells. Bioelectrochemistry 2004;62:107-113.

[37] Mohandas N, Gascard P. What do mouse gene knockouts tell us about the structure and function of the red cell membrane?. Bailliere's Best Practice and Research in Clinical Haematology 1999;12:605-620.

[38] Kamruzzahan ASM, Kienberger F, Stroh CM, Berg Jö, Huss R, Ebner A, et al. Imaging morphological details and pathological differences of red blood cells using tapping-mode AFM. Biol Chem 2004;385:955-960.

[39] Kostić IT, Ilić VL, Đorđević VB, Bukara KM, Mojsilović SB, Nedović VA, et al. Erythrocyte membranes from slaughterhouse blood as potential drug vehicles: Isolation by gradual hypotonic hemolysis and biochemical and morphological characterization. Colloids and Surfaces B: Biointerfaces 2014;122:250-259.

[40] Gutiérrez Millán C, Castañeda AZ, Sayalero Marinero ML, Lanao JM. Factors associated with the performance of carrier erythrocytes obtained by hypotonic dialysis. Blood Cells, Molecules, and Diseases 2004;33:132-140.

[41] Hamidi M, Tajerzadeh H. Carrier erythrocytes: an overview. Drug Deliv 2003;10:9-20.

[42] Dale G, Villacorte D, Beutler E. High-yield entrapment of proteins into erythrocytes. Biochem Med 1977;18:220-225.

[43] Weaver JC, Chizmadzhev YA. Theory of electroporation: A review. Bioelectrochem Bioenerget 1996;41:135-160.

[44] Bliss JG, Harrison GI, Mourant JR, Powell KT, Weaver JC. Electroporation: The population distribution of macromolecular uptake and shape changes in red blood cells following a single 50 μs square wave pulse. Bioelectrochem Bioenerget 1988;20:57-71.

[45] Shi J, Kundrat L, Pishesha N, Bilate A, Theile C, Maruyama T, et al. Engineered red blood cells as carriers for systemic delivery of a wide array of functional probes. Proc Natl Acad Sci U S A 2014;111:10131-10136.

[46] HOFFMAN JF. Physiological characteristics of human red blood cell ghosts. J Gen Physiol 1958;42:9-28.

[47] Amrutkar RD, Vyawahare TG, Bhambar RS. Resealed erythrocytes as targeted drug delivery system. International Journal of Pharmaceutical Research 2011;3:10-18.

[48] Cremel M, Guérin N, Horand F, Banz A, Godfrin Y. Red blood cells as innovative antigen carrier to induce specific immune tolerance. Int J Pharm 2013;443:39-49.

[49] Fan W, Yan W, Xu Z, Ni H. Erythrocytes load of low molecular weight chitosan nanoparticles as a potential vascular drug delivery system. Colloids and Surfaces B: Biointerfaces 2012;95:258-265.

[50] Millán CG, Marinero MLS, Castañeda AZ, Lanao JM. Drug, enzyme and peptide delivery using erythrocytes as carriers. J Controlled Release 2004;95:27-49.

[51] Muzykantov VR. Drug delivery by red blood cells: Vascular carriers designed by mother nature. Expert Opinion on Drug Delivery 2010;7:403-427.

[52] Rao KT, Prabha KS, Prasanna PM. Resealed erythrocytes: As a specified tool in novel drug delivery carrier system. Research Journal of Pharmaceutical, Biological and Chemical Sciences 2011;2:496-512.

[53] Serafini S, Rossi L, Antonelli A, Fraternale A, Cerasi A, Crinelli R, et al. Drug delivery through phagocytosis of red blood cells. Transfusion Medicine and Hemotherapy 2004;31:92-101.

[54] Shaillender M, Luo R, Venkatraman SS, Neu B. Layer-by-layer microcapsules templated on erythrocyte ghost carriers. Int J Pharm 2011;415:211-217.

[55] Kim S-, Kim E-, Hou J-, Kim J-, Choi H-, Shim C-, et al. Opsonized erythrocyte ghosts for liver-targeted delivery of antisense oligodeoxynucleotides. Biomaterials 2009;30:959-967.

[56] Yamagata K, Kawasaki E, Kawarai H, Iino M. Encapsulation of Concentrated Protein Into Erythrocyte Porated by Continuous-Wave Ultrasound. Ultrasound in Medicine and Biology 2008;34:1924-1933.

[57] Katz U, Lancaster J-, Ellory JC. Hypotonic-induced transport pathways in Xenopus laevis erythrocytes: Taurine fluxes. Comparative Biochemistry and Physiology - A Molecular and Integrative Physiology 2003;134:355-363.

[58] Piatti E, Piacentini MP, Fraternale D, Bucchini A, Mangani F, Accorsi A. myo-[3H]-inositol loaded erythrocytes and white ghosts: Two models to investigate the phosphatidylinositol synthesis in human red cells. Biochimie 1999;81:1011-1014.

[59] Briones E, Colino Clara I. CI, Lanao JM. Study of the factors influencing the encapsulation of zidovudine in rat erythrocytes. Int J Pharm 2010;401:41-46.

[60] Briones E, Colino CI, Millán CG, Lanao JM. Increasing the selectivity of amikacin in rat peritoneal macrophages using carrier erythrocytes. European Journal of Pharmaceutical Sciences 2009;38:320-324.

[61] Lotero LA, Olmos G, Diez JC. Delivery to macrophages and toxic action of etoposide carried in mouse red blood cells. Biochimica et Biophysica Acta - General Subjects 2003;1620:160-166.

[62] Sanz S, Lizano C, Luque J, Pinilla M. In vitro and in vivo study of glutamate dehydrogenase encapsulated into mouse erythrocytes by a hypotonic dialysis procedure. Life Sci 1999;65:2781-2789.

[63] Hamidi M, Zarrin AH, Foroozesh M, Zarei N, Mohammadi-Samani S. Preparation and in vitro evaluation of carrier erythrocytes for RES-targeted delivery of interferon-alpha 2b. Int J Pharm 2007;341:125-133.

[64] Doberstein S, Wiegand G, Machesky L, Pollard T. Fluorescent erythrocyte ghosts as standards for quantitative flow cytometry. Cytometry 1995;20:14-18.

[65] Ahn S, Jung SY, Seo E, Lee SJ. Gold nanoparticle-incorporated human red blood cells (RBCs) for X-ray dynamic imaging. Biomaterials 2011;32:7191-7199.

[66] Brähler M, Georgieva R, Buske N, Müller A, Müller S, Pinkernelle J, et al. Magnetite-loaded carrier erythrocytes as contrast agents for magnetic resonance imaging. Nano letters 2006;6:2505-2509.

[67] Gopal V, Kumar AR, Usha N, Karthik A, Udupa N. Effective drug targeting by erythrocytes as carrier systems. Curr.Trends Biotechnol.Pharm 2007;1:18-33.

[68] Donadee C, Raat NJ, Kanias T, Tejero J, Lee JS, Kelley EE, et al. Nitric oxide scavenging by red blood cell microparticles and cell-free hemoglobin as a mechanism for the red cell storage lesion. Circulation 2011;124:465-476.

[69] Lion N, Crettaz D, Rubin O, Tissot J. Stored red blood cells: A changing universe waiting for its map(s). Journal of Proteomics 2010;73:374-385.

[70] Chin-Yee I, Arya N, d'Almeida MS. The red cell storage lesion and its implication for transfusion. Transfus Sci 1997;18:447-458.

[71] Chambers E, Mitragotri S. Prolonged circulation of large polymeric nanoparticles by non-covalent adsorption on erythrocytes. J Controlled Release 2004;100:111-119.

[72] Doshi N, Zahr AS, Bhaskar S, Lahann J, Mitragotri S. Red blood cell-mimicking synthetic biomaterial particles. Proceedings of the National Academy of Sciences 2009;106:21495-21499.

[73] Merkel TJ, Jones SW, Herlihy KP, Kersey FR, Shields AR, Napier M, et al. Using mechanobiological mimicry of red blood cells to extend circulation times of hydrogel microparticles. Proc Natl Acad Sci U S A 2011;108:586-591.

[74] Haghgooie R, Toner M, Doyle PS. Squishy non-spherical hydrogel microparticles. Macromolecular Rapid Communications 2010;31:128-134.

[75] Kinosita Jr K. Survival of sucrose loaded erythrocytes in the circulation. Nature 1978;272:258-260.

[76] Moroz VV, Chernysh AM, Kozlova EK, Borshegovskaya PY, Bliznjuk UA, Rysaeva RM, et al. Comparison of red blood cell membrane microstructure after different physicochemical influences: Atomic force microscope research. J Crit Care 2010;25:539.e1-539.e12.

[77] Bustamante López SC, Meissner KE. Characterization of carrier erythrocytes for biosensing applications. J Biomed Opt 2017;22:091510-091510.

[78] Betz T, Bakowsky U, Müller MR, Lehr C, Bernhardt I. Conformational change of membrane proteins leads to shape changes of red blood cells. Bioelectrochemistry 2007;70:122-126.

[79] Phua KK, Boczkowski D, Dannull J, Pruitt S, Leong KW, Nair SK. Whole Blood Cells Loaded with Messenger RNA as an Anti-Tumor Vaccine. Advanced healthcare materials 2013.

[80] Mouneimne Y, Tosi P, Gazitt Y, Nicolau C. Electro-insertion of xeno-glycophorin into the red blood cell membrane. Biochem Biophys Res Commun 1989;159:34-40.

[81] Deloach JR. Carrier erythrocytes. Med Res Rev 1986;6:487-504.

[82] DeLoach JR. Encapsulation of exogenous agents in erythrocytes and the circulating survival of carrier erythrocytes. J Appl Biochem 1983;5:149-157.

[83] Thanh NT. Magnetic Nanoparticles: From Fabrication to Clinical Applications CRC press; 2012.

[84] Sternberg N, Georgieva R, Duft K, Bäumler H. Surface-modified loaded human red blood cells for targeting and delivery of drugs. J Microencapsul 2012;29:9-20.

[85] Zimmermann U, Pilwat G, Vienken J. Erythrocytes and Lymphocytes as Drug Carrier Systems: Techniques for Entrapment of Drugs in Living Cells. In: Anonymous Cancer Chemo-and Immunopharmacology, Springer; 1980, p. 252-259.

[86] Jordan CA, Neumann E, Sowers AE. Electroporation and Electrofusion in Cell Biology Springer Science & Business Media; 2013.

[87] Gruber W, Deuticke B. Comparative aspects of phosphate transfer across mammalian erythrocyte membranes. J Membr Biol 1973;13:19-36.

[88] Schwister K, Deuticke B. Formation and properties of aqueous leaks induced in human erythrocytes by electrical breakdown. Biochimica et Biophysica Acta (BBA)-Biomembranes 1985;816:332-348.

[89] Roland L, Drillich M, Iwersen M. Hematology as a diagnostic tool in bovine medicine. Journal of Veterinary Diagnostic Investigation 2014.

[90] Latimer KS. Duncan and Prasse's Veterinary Laboratory Medicine: Clinical Pathology John Wiley & Sons; 2011.

[91] Safeukui I, Buffet PA, Deplaine G, Perrot S, Brousse V, Ndour A, et al. Quantitative assessment of sensing and sequestration of spherocytic erythrocytes by the human spleen. Blood 2012;120:424-430.

[92] Samsel L, McCoy Jr. JP. Imaging flow cytometry for the study of erythroid cell biology and pathology. J Immunol Methods 2015;423:52-59.

[93] Zimmermann U. Cellular drug-carrier systems and their possible targeting. Targeted Drugs 1983:153-200.

[94] Baker RF. Entry of ferritin into human red cells during hypotonic haemolysis 1967.

[95] Lewis D. Red blood cells for drug delivery. Pharm.J 1984;233:384-385.

[96] Acker JP, M. Croteau I, Yi Q. An analysis of the bias in red blood cell hemolysis measurement using several analytical approaches. Clinica Chimica Acta 2012;413:1746-1752.

[97] Stadler AM, Digel I, Artmann GM, Embs JP, Zaccai G, Büldt G. Hemoglobin Dynamics in Red Blood Cells: Correlation to Body Temperature. Biophys J 2008;95:5449-5461.

[98] Liu SC, Yi SJ, Mehta JR, Nichols PE, Ballas SK, Yacono PW, et al. Red cell membrane remodeling in sickle cell anemia. Sequestration of membrane lipids and proteins in Heinz bodies. J Clin Invest 1996;97:29-36.

[99] Rechsteiner M. Uptake of proteins by red blood cells. Exp Cell Res 1975;93:487-492.

[100] Kravtzoff R, Ropars C, Laguerre M, Muh J, Chassaigne M. Erythrocytes as carriers for L-asparaginase. Methodological and mouse in-vivo studies. J Pharm Pharmacol 1990;42:473-476.

[101] Pitt E, Johnson CM, Lewis DA, Jenner DA, Offord RE. Encapsulation of drugs in intact erythrocytes: an intravenous delivery system. Biochem Pharmacol 1983;32:3359-3368.

[102] Nuttall AL. Techniques for the observation and measurement of red blood cell velocity in vessels of the guinea pig cochlea. Hear Res 1987;27:111-119.

[103] Biagiotti S, Paoletti MF, Fraternale A, Rossi L, Magnani M. Drug delivery by red blood cells. IUBMB Life 2011;63:621-631.

[104] Magnani M, Pierig F, Rossi L. Erythrocytes as a novel delivery vehicle for biologics: From enzymes to nucleic acid-based therapeutics. Therapeutic Delivery 2012;3:405-414.

[105] Chiarantini L, Rossi L, Fraternale A, Magnani M. Modulated red blood cell survival by membrane protein clustering. Mol Cell Biochem 1995;144:53-59.

[106] Antonelli A, Sfara C, Battistelli S, Canonico B, Arcangeletti M, Manuali E, et al. New strategies to prolong the in vivo life span of iron-based contrast agents for MRI. PloS one 2013;8:e78542.

[107] Magnani M, Chiarantini L, Vittoria E, Mancini U, Rossi L, Fazi A. Red blood cells as an antigen-delivery system. Biotechnol Appl Biochem 1992;16:188-194.

[108] Antonelli A, Magnani M. Red blood cells as carriers of iron oxide-based contrast agents for diagnostic applications. Journal of biomedical nanotechnology 2014;10:1732-1750.

[109] Magnani M, Rossi L, Brandi G, Schiavano GF, Montroni M, Piedimonte G. Targeting antiretroviral nucleoside analogues in phosphorylated form to macrophages: in vitro and in vivo studies. Proc Natl Acad Sci U S A 1992;89:6477-6481.

[110] Flower R, Peiretti E, Magnani M, Rossi L, Serafini S, Gryczynski Z, et al. Observation of erythrocyte dynamics in the retinal capillaries and choriocapillaris using ICG-loaded erythrocyte ghost cells. Invest Ophthalmol Vis Sci 2008;49:5510-5516.

[111] Bahmani B, Bacon D, Anvari B. Erythrocyte-derived photo-theranostic agents: hybrid nano-vesicles containing indocyanine green for near infrared imaging and therapeutic applications. Scientific reports 2013;3.

[112] Safeukui I, Buffet PA, Perrot S, Sauvanet A, Aussilhou B, Dokmak S, et al. Surface area loss and increased sphericity account for the splenic entrapment of subpopulations of Plasmodium falciparum ring-infected erythrocytes. PLoS One 2013;8:e60150.